Journal of Applied Fluid Mechanics, Vol. 17, No. 10, pp. 2245-2265, 2024.
Available online at www.jafmonline.net, ISSN 1735-3572, EISSN 1735-3645.
https://doi.org/10.47176/jafm.17.10.2521

Investigations on Design Space for Highly Loaded Tandem Bladed Axial Flow Rotor- novel Stator for Low-speed Compressor Research Facility

A. Singh and C. S. Mistry†

Department of Aerospace Engineering, Indian Institute of Technology, Kharagpur, West Bengal, 721302, India

†Corresponding Author Email: csmistry@aero.iitkgp.ac.in

ABSTRACT

Tandem bladed axial flow compressor concept has immense potential for increasing the stage loading over conventional stages. This infers significant improvement in gas turbine engine operational economics and performance. However, implementation of tandem configuration invites additional three dimensionalities in the flow field. This complicates the design process limiting the realization of the tandem bladed rotor concept. The present study addresses the strategies for development of a low-speed axial compressor design implementing tandem bladed rotor and single stator. Both the rotor and stator flow mechanisms have been investigated in detail using steady state simulations. A highly loaded tandem bladed rotor is followed by single bladed stator which handles the highly swirled flow. The single blade configuration of stator results in higher diffusion factor which is more susceptible to the flow separation. Moreover, a dual wake structure evolves through the rotor passage due to highly loaded individual blades. The stage design follows an unconventional approach of tandem rotor-single stator over the reported tandem rotor-tandem stator or only tandem bladed stator configuration. The aerodynamic match between the tandem bladed rotor and stator has been of critical importance in development of this design. The rotor has been designed for highest possible energization of flow by fine tuning the variation of tandem nozzle geometry throughout the span to complement the intended loading profile. The stator is aimed at letting the flow pass through with a chordwise varying diffusion profile. The novelty of the work lies in discussion of tandem rotor and single bladed stator flow physics altogether highlighting the interdependence of decision-making process for both.

Article History

Received December 20, 2023
Revised April 10, 2024
Accepted April 28, 2024
Available online July 31, 2024

Keywords:

Tandem rotor
DCA Camber
Vortex breakdown
Tip clearance
Flow blockage

1. Introduction

Modern gas turbine engines have evolved through the state of the art research and development seeking consistent improvement in power and efficiency. The current trend in engine research dictates the requirement of compact engine sizes as a primary need. The overall engine size is significantly influenced by the length of the compressor for a given pressure rise. The overall length of an axial flow compressor can be reduced by reducing the total number of stages for the same work capacity. The conventional axial flow compressors are prone to flow separation due to adverse pressure gradients upon higher aerodynamic loading which limits the selection of number of stages. The requirement of high aerodynamic loading per stage with permitted losses can be achieved by unconventional design strategies. Tandem bladed axial compressors have shown potential for being such an alternative option to serve the aforementioned purpose. A significant amount of effort has been made in the development and understanding of tandem blade concept. A tandem bladed rotor consists of two different blades mounted on a single rotor to attain the required flow turning. The basic concept of tandem arrangement against a conventional single blade is shown in Fig. 1.

The aerodynamic leverage offered by tandem configuration is based on two effects. The first being increase of circulation (blade loading) around the fore blade due to the downstream presence of the aft blade. The second effect is the re-energization of the suction surface boundary layer achieved by the nozzle flow emerging from the inter-blade gap (Fig. 1b). Together, these two

Nomenclature

C	chord	P_{local}	local static pressure
U	rotor speed	P_0	total Pressure
a	axial spacing	DF	Diffusion Factor
s	pitch (unit: mm)	ω	total pressure loss coefficient
t	pitch wise spacing	C_p	coefficient of pressure
FB	Fore Blade	DOR	Degree of Reaction
AB	Aft Blade	LS	Load Split
PP	Percent Pitch	C_a	axial velocity
AO	Axial Overlap	σ	solidity
$\vec{\xi}$	Abs vorticity vector	ψ	stage loading coefficient, $\Delta P_0/\rho U_m^2$
$\vec{V}$	velocity vector	φ	flow coefficient, C_a/U_m
ω	loss Coefficient, $(\overline{P_{01}} - P_0)/{}^1/_2\,\rho V^2$	**Suffix**	
θ	camber	*1*	fore blade
γ	stagger	*2*	aft blade
β	flow angles	*11*	fore blade LE
$\Delta\beta$	deflection	*22*	aft blade TE
ρ	density	*T*	tandem
P_{ref}	reference static pressure	*m*	mean span
C_p	coefficient of pressure, $(P_{local} - P_{ref})/{}^1/_2\,\rho {C_a}^2$	*t*	tip span

make the tandem configuration a passive flow control mechanism enabling higher fluid deflection than conventional blading. The application of tandem blading concept in compressor design was demonstrated in the report by Spraglin (1951) in the early 50's. The earliest prototype developed with a tandem bladed rotor was designed and tested by Sheets (1955). A rotor efficiency of 94% with permitted losses as per the then standards was reported by the author. Sangers (1971) conducted an exhaustive study on various parameters of tandem configuration and claimed promising potential for future development of tandem cascades. Bammert et al. (Bammert & Beelte, 1980; Bammert & Staude, 1981) designed and successfully tested the three-stage axial flow compressor incorporating tandem blading on rotor. Authors reported 18% less losses at design point in comparison to a conventional rotor. In recent time, McGlumpy et al. (2010) and Falla (2004) examined the performance of subsonic tandem configuration against conventional blade arrangement. Recently Madasseri Payyappalli and Pradeep (2018) introduced the tandem rotor configurations as first rotor in a low-speed contra rotating fan. Authors reported improved performance with a reduction in operating range limited by the tandem rotor. The recent interests in high speed compressor designs have led to investigations on tandem bladed rotors in transonic fan applications. Sakai et al. (2003) have designed and tested the transonic tandem compressor fan with a pressure ratio of 2.2. The authors reported overall stage performance based on 2-D plots with less emphasis on flow physics as a whole. Mohsen et al. (2017) designed and numerically tested a parametrically optimized tandem rotor with similar inflow conditions to 'ROTOR 37'. A 17% increase in total pressure ratio with 2% improvement in adiabatic efficiency has been reported at the design point. The complex shock induced flow characteristics have been addressed by Tao et al. (2020) for a tandem rotor with an inflow Mach no. of 1.2. The authors proposed unconventional specifically optimized airfoils for transonic tandem applications owing to chaotic aerodynamic interactions between both airfoils. Zhou et al. (Zhou et al., 2023) proposed a novel transonic partial-span tandem fan concept for enhancing the work capacity near the fan's core. Both flow capacity and pressure ratio were enhanced by 6.1% and 20% respectably in comparison to the baseline case. The aforesaid transonic tandem investigations are centered around high speed fan applications with major emphasis on management of shock induced phenomena.

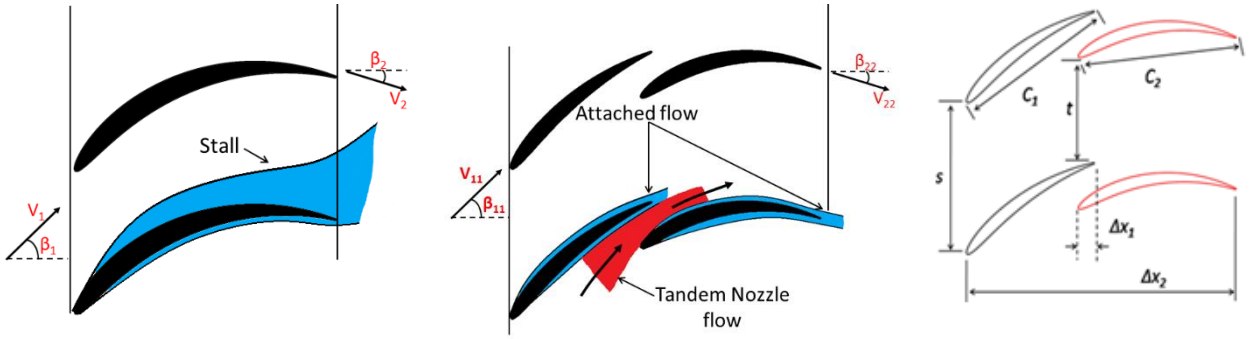

(a) Conventional Blade (b) Tandem Blade (c) Tandem geometry

Fig. 1 Conventional and tandem bladed geometry

The flow field inside a tandem compressor is more complex owing to three-dimensional effects and seeks additional concern for design and development. As a known practical application, tandem cascades have been implemented as a stator for GE J-179 compressor.

A schematic of tandem configuration along with associated geometric parameters is shown in Fig. 1(c).

$$AO = \Delta x_1/\Delta x_2 \tag{1}$$

$$PP = t/s \tag{2}$$

The recommended geometrical features in terms of axial overlap (AO) and percentage pitch (PP) [Equations (1) and (2)] for published tandem designs lie in a narrow envelope which varies slightly as per design approach. McGlumphy et al. (2010) varied the AO in the range -10% to 10% and reported least losses for 0% AO. Likewise Schneider and Kožulović (2013) reported the performance of subsonic tandem cascade and confirmed optimum performance at 19% AO based on true chord. The tandem cascade study by Madasseri Payyappalli and Shine (2015) performed optimally at zero AO. The insightful investigation by Bammert and Staude (1980, 1981) focusses primarily on optimization of rotor geometry for minimal losses while maintaining a high stage degree of reaction. This relieved the stator loading (Bammert & Ahmadi, 1978) and was a crucial design feature to realize the 3-stage tandem rotor compressor design. Eshraghi et al. (2014) on the other hand resorted to tandem rotor-tandem stator configuration. The study focused on overall stage performance and limited design aspects were discussed in detail. It is evident that application of tandem configuration is centered around stator applications. The available literature reports focus on the individual performance of tandem stator cascades or transonic tandem bladed rotors. The integration of tandem rotor concept as a core compressor stage for a gas turbine engine application is based on its performance under stage configuration. A feasible stage application of this passive flow control concept requires an understanding of flow physics in a stage environment – tandem rotor-single stator combination as a whole rather than an isolated entity. The present paper addresses the design approach of a *tandem bladed rotor-single bladed stator* stage with a moderate degree of reaction for *low-speed university research facility*. The authors have reasons to believe that the passive flow control benefit offered by tandem geometry can be harnessed more efficiently in a dynamic environment. The purpose of the current study is to delineate the design features in a conventional stage design configuration rather than focusing on tandem rotor or only tandem stator configuration. The strategies for selection of various geometric parameters have been described in the light of flow physics based on numerical study. This necessitates the description of design strategies for tandem bladed rotor as well as stator simultaneously.

Though the performance of rotor-stator combination as stage is interdependent, the authors have managed to segregate the decision making process in order to organize the design space for this unique stage configuration. Following broad queries constitute the layout of this contribution -

1. What should be the aero-thermodynamic design methodology to begin for tandem rotor and single stator configuration?
2. How should the aerodynamic load between fore and aft blade be distributed for tandem bladed rotor?
3. What should be the systematic selection procedure for parameters like axial overlap (AO) and percentage pitch (PP) (along with their spanwise variation) for the tandem rotor?
4. What should be the appropriate tip profile for rotor blades which results in a constant tip gap for whole rotor as single entity?
5. Will there be any effect of change of AO and PP near the tip region? How will the tip clearance flow and endwall boundary layer interact for tandem rotor configuration?
6. The twin wake system from rotor makes the design criteria for the downstream stator more challenging and unique. What is the evolution pattern of the twin wake system along with tip clearance-endwall flow resulting in a highly 3-dimensional flow structure faced by the downstream stator?
7. The benefit of higher fluid deflection in rotor results in higher flow deflection angles for stator as well. The motive of higher pressure rise per stage can be severely penalized as aerodynamic limitations of stator come into the picture. What should be the central idea of design of such stator to meet this special requirement?

The above issues are highly intertwined and need to be addressed collectively to give a broader picture. The first four questions are design and designer's choices motivated by existing literature and the latter three questions are based on the resulting flow features. The increased structural complexity is halfway justified with higher end wall losses. The available literatures discuss primarily the effect of axial spacing on the overall flow field. Very limited discussion on strategies for selection of axial overlap for variable spanwise loading is available in open literature. Hence a systematic numerical study to understand the flow physics by varying axial overlap between tandem blades from hub to tip with a constant percentage pitch was conducted to come up with guidelines for selection of overlap.

On a different note, the realization of compressor stage depends on the performance of rotor as well as stator. The higher fluid deflection facilitated by tandem rotor becomes a major challenge for the downstream stator. Aerodynamic and economic constrains dissuade the implementation of tandem rotor-tandem stator configuration. The work potential of tandem bladed rotor can be seriously compromised due do an incompatible stator. Hence the impact of tandem exit flow field on flow physics of evolving stator design is important and has been discussed in detail.

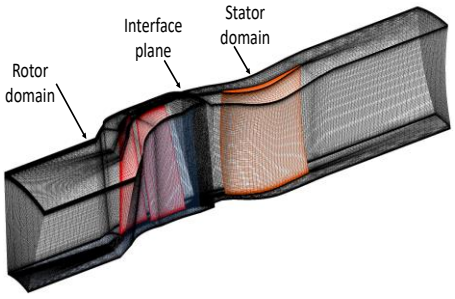

(a) Computational domain

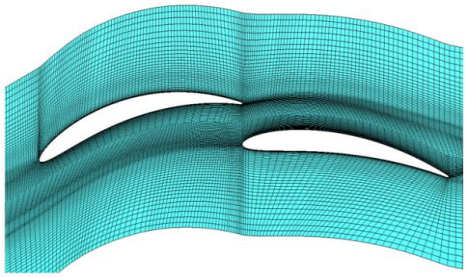

(b) Computational mesh at 50% span

Fig. 2 Computational domain and mesh distribution

2. COMPUTATIONAL STUDY AND DOMAIN DISCRETIZATION

The computational domain consists of four parts - an inlet, a rotational domain, the stator and exit domain (Fig. 2a). The inlet domain begins from one -rotor chord upstream of rotor and the exit domain continued till 2-chord downstream of stator trailing edge. The computational domain is discretized using ANSYS TurboGrid®. A multi-block structured grid with hexagonal elements has been implemented for computation. The generated mesh consists of ~3 million elements in each rotor and stator domain. A y^+ value of 1 is maintained along all the wall boundaries in order to capture the boundary layer profile. An O-grid with 70 spanwise elements (excluding tip clearance) has been implemented throughout the span. Additional 60 elements are included in the hub and shroud boundary layers which result in an endwall expansion ratio of ~1.15 and overall 130 elements along blade span. Figure 2(a, b) show the mesh distribution as a whole and at constant span respectively. The orthogonal element distribution in the O-grid is about 16-18 for the rotor as well as stator. A tip clearance of 3 mm (3% of span) has been proposed for both the blades. The range is typical for low speed designs under allowable manufacturing capabilities and has been modeled in the computational study. In order to capture the tip clearance flow with intended spatial resolution the mesh is refined additionally in the tip region by using 55-60 elements for each blade. Out of which 30-45 elements are of constant size which results into an effective expansion ratio of 1.08 in the tip region. The commercially available solver ANSYS CFX® is used for solving the steady-state Reynolds Averaged Navier Strokes equations (RANS). Belamri et al. (2005a, b) demonstrated the robustness of CFX® for capturing the flow physics with manageable computational resources. A uniform pressure profile representing atmospheric pressure is imposed on

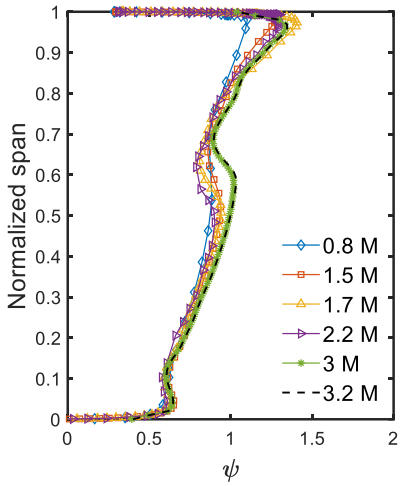

Fig. 3 Loading coefficient for different mesh sizes

the inlet boundary. The two equation shear stress transport (SST) model is used for modeling turbulence to efficiently capture the vortices in near surface flows in adverse pressure gradient regime (Wilcox, 2006). The mesh sensitivity analysis was performed to rule out any discrepancies arising due to inconsistent mesh quality. The stage consists of highly loaded tandem bladed rotor which entails important tip clearance related flow phenomena. It is obligatory to eliminate mesh dependency in the tip region as important tip clearance–endwall flow interactions need to be addressed. The mesh sensitivity study was performed by adjusting both global as well as tip region mesh element distribution carefully. The result of the mesh refinement study is shown in Fig. 3 in terms of spanwise stage loading coefficient. Accordingly, 3.2 million elements were finalized for all the further studies as distribution of both global and local flow properties become invariant. One of the primary objectives were to capture the interaction of rotor wakes and tip clearance flow with stator. A comparison of available interface modelling techniques for turbomachinery simulations can be referred from the dedicated study by Corsini et al (2013). The rotor-stator interface was modelled using frozen rotor interface' as it preserves the rotor exit non-uniformities to maximum extent.

3. SELECTION OF GEOMETRICAL PARAMETERS FOR THE DESIGN OF TANDEM ROTOR BLADES

The primary goal of the present study is to systematize the stage design methodology for the tandem rotor –single stator compressor stage. The practical applications of tandem blading for axial flow compressors are limited to stators due to aerodynamic constraints and mechanical challenges. With an increased understanding of tandem blading flow physics, the authors believe that tandem rotors may perform equally well both as individual rotor as well as in stage configuration. A low speed tandem bladed compressor is designed to achieve an overall stage total pressure rise of 1400 Pa and mass flow rate of 3.75 kg/s. The targeted high flow coefficient is

Table 1 Design parameters of rotor blades for base case

Stage Total Pressure Rise	1400 Pa
Design Rotational Speed	2400 RPM
Rotor Tip Diameter	400 mm
hub-to-tip ratio	0.5
Rotor aspect ratio (effective)	1.0
Stator Aspect ratio	0.9

motivated by the logic to arrive at a stage with high mass flow rate per unit frontal area. The various design parameters of the stage are summarized in Table 1. The 2-D design rule proposed by McGlumpy et al. (2010) has been implemented for design of baseline tandem bladed rotor. The simple design rule assumes independent operation of individual airfoils and the equivalent diffusion factor for the tandem airfoil is given by

$$D_T = 1 - \frac{\cos\beta_{11}}{\cos\beta_{22}} + \frac{\cos\beta_{11} \times (\tan\beta_{11} - \tan\beta_{22})}{2\sigma_{eff}} \quad (3)$$

The diffusion factor for individual blades is calculated by substituting appropriately for the inlet and exit angles respectively. The relative air inlet angle for the aft blade has been assumed equal to the relative air exit angle from the fore blade. The simple design rule is an efficient tool to design the blading owing to its simplicity. However as discussed in the following sections the mutual independence is unrealistic along the span and especially in the tip region due to the interaction of tip clearance flows and endwall boundary layers. The increased aerodynamic loading in the tip region results in two distinct stronger wakes which carry the legacy of respective blades in terms of flow angles. For tandem configuration, the geometrical parameters such as Axial Overlap (*AO*) and Percent Pitch (*PP*) are defined by equations (1) and (2) with respect to Fig. 1(c). The aerodynamic design consists of a controlled spanwise loading distribution targeted to achieve the maximum possible pressure rise coefficient.

4. AERODYNAMIC LOAD DISTRIBUTIONS FOR TANDEM ROTOR BLADES

The aerodynamic load split between fore and aft blade of tandem rotor configuration can be expressed in various ways –*based on camber ratio, chord ratio and appropriate diffusion factor ratio*. The selection of load split method is trivial but quantitatively the load split plays a pivotal role in the overall performance and operating range of the compressor stage. The load split in the current study is *an aerodynamic load split* resulting in the distribution of turning between the fore and the aft blade. The actual load split depends on relative location of aft blade to fore blade as well as the prescribed aerodynamic load split. The relative location in the present context is characterized by axial overlap and percentage pitch which are based on numerous design iterations. The load split has considerable influence on the end-wall losses as well. The investigations of end wall flow phenomena for tandem bladed compressors are not that comprehensive as that for conventional axial flow compressors. The 3-dimensional flow fields near the end walls in tandem cascade have been studied in detail by McGlumpy et al. (2010). The endwall losses of a tandem cascade as a consequence of load split were investigated by Schluer et al. (2009). Bohle and Frey (2014) conducted a detailed numerical and experimental evaluation of effect of overall turning and load split on the sidewall flow structure of tandem cascade. The authors reported significant three dimensional flow structures near end walls. The authors claimed that Lei's (Lei et al., 2018) criteria is skeptical for predicting the wall stall in case of tandem cascade. The load split on both the blades is defined [Eq. 4] as the ratio of DF for fore blade to the summation of DF for both blades.

$$LS = \frac{DF_1}{DF_1 + DF_2} \quad (4)$$

For present design the aerodynamic load was distributed such that the fore blade is highly loaded as compared to aft blade. The decision for uneven loading is based on the logical strategy of aft airfoil receiving a pre-conditioned flow from the fore airfoil. The incidence tolerance of the aft blade is assisted by nozzle gap flow. The loading is relaxed on the aft blade in order to accommodate the incoming flow from the fore blade during off design operation and this helps in extending the overall operating range. The British C4 airfoil was implemented for generation of blades owing to its proved reliability in low to moderate Mach number flows (Alm-Eldien, 2015). The blade stacking for fore blade has been done about centre of gravity (CG) to comply with structural requirements. The aft blade however has been stacked in accordance with required axial overlap and percentage pitch variation along the span. Thus, the stacking of the aft blade is a trade-off between the recommended structural and required aerodynamic constrains. The decision-making process for stacking was favoured by the selected low aspect ratio configuration which is in line to HP compressor stage requirements. For the present design the aerodynamic loading was selected such that the tip is highly loaded and hub is moderately loaded for both the rotor blades. The low-speed design requirement results in higher blade curvature at the hub which is more prone to flow separation. In order to avoid such possibilities, the blade loading has been relaxed at the hub and compensated for by increasing the loading at the tip. For such requirement the AO plays important role and hence it has been varied accordingly to assist in higher turning in the tip region for rotor.

5. SELECTION OF AXIAL OVERLAP AND PERCENTAGE PITCH FOR TANDEM ROTOR

During initial design phase the axial overlap (AO) and percentage pitch (PP) were selected based on the available literature on tandem cascades-the major recommendations

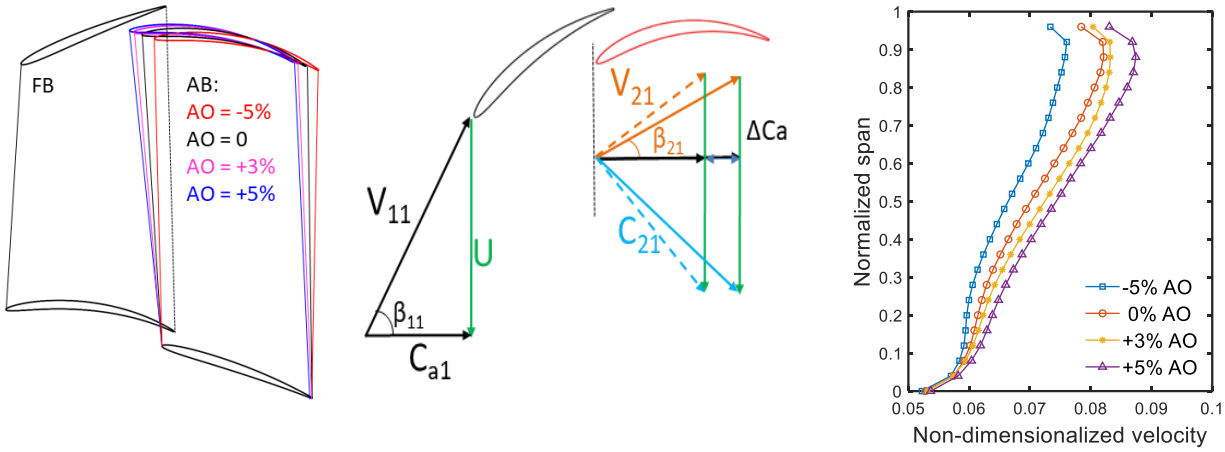

(a) Rotor geometries analyzed (b) Effect of tandem configuration on local velocity triangle (c) Effect of Axial overlap on velocity through the nozzle gap

Fig. 4 Effect of AO on velocity triangle

were low AO and high PP (Sanger, 1971, 1973; Bammert & Staude, 1980; McGlumphy et al., 2010). With a number of design iterations 0% AO and 82% PP have been arrived at as parameters for the base case. The main goal for the initial design was to achieve the best possible performance in terms of expected pressure rise with minimum losses. The effect of axial overlap (AO) is taken into account by treating both airfoils as a single airfoil. The computational study was carried out to study the effect of axial overlap (0% at the hub and 0%, -5%, +5%, +3% of effective chord near the tip) on the overall flow structure along the span with special consideration on tip clearance flow structure. As mentioned earlier, the tandem configuration acts as a passive aerodynamic flow control mechanism. Hence a change in AO results in change of aerodynamic loading on both the airfoils due to change of circulation and re-energization of boundary layer flow. Based on numerical study it was found that the tip clearance flow field and losses along the span are very sensitive to aerodynamic blade loading and thus AO. The rational for varying the axial overlap from hub to tip is motivated by the targeted spanwise loading distribution which increases from hub to tip. Thus, it clearly necessitates the need of a higher tandem nozzle action in the upper span regions dictating increase in axial overlap. The resulting rotor geometries based on selected AO variations are depicted in Fig.4(a). It should be noted that the changes in AO are brought about by changing the stacking line of aft blade only. As discussed earlier, in order to incorporate the need for changes in axial overlap between the blades, the aft blade profiles cannot be stacked about the CGs lying along radial line. To harness the aerodynamic benefits of tandem configuration a controlled AO and PP distribution across the span is a must and so the stacking line for aft blade often becomes inclined if not curved. The three-dimensional profile stacking in not uncommon for stators but it is structurally challenging for a rotor blade. The present study is targeted for a tandem rotor test rig development which raises concern for such strategic blade stacking method. The low-speed design approach was primarily motivated to provide some relief in this aspect as it reduces the bending stresses induced due to three-dimensional blade stacking. In order to handle this issue tactfully, instead of varying both the AO and the PP, only AO was varied (considering PP to be constant) to reduce the blade three-dimensionality.

Authors believe that changing both the geometrical parameters would have resulted in a better aerodynamic design but at the cost of severe structural compromise. The structural changes in individual blade shapes are similar to sweep and dihedral respectively. Changing the AO to -5% and +5% actually changes the aft blade sweep from backward to forward respectively. The change of axial overlap is supposed to change the fore blade loading as anticipated by the potential flow theory. An overall effect of tandem blading can be explained by velocity triangles for individual blades (Fig. 4b). Although both the blades work in unison in order to produce the desired work output, in effect there are two distinct airfoils operating individually. This implies two velocity triangles. The tandem nozzle effect results in local increase of axial velocity near the LE of aft airfoil (ΔC_a) which results in decrease of incidence for the aft blade. This local decrease of incidence holds the potential for better performance at off-design. The choice of -5%, 0% and +5% AO selected in the present study are representative of typical values selected in applications of tandem blading (Bammert & Staude, 1981; McGlumphy et al., 2009; Hoeger et al., 2011; Hergt & Siller, 2019).

Based on number of iterations it was found that AO of 3% serves as the best case as per the discussion in the dedicated study (Singh & Mistry, 2019). The effect of change of axial overlap has a major influence on tandem nozzle velocity as it affects the formation of nozzle shape due to variation in spacing along the span. Figure 4(c) shows the spanwise distribution of normalized velocity through the tandem nozzle at nozzle exit plane for the four axial overlaps considered. The velocity through the tandem nozzle increases as the axial overlap increases from hub to shroud. It can be observed that maximum nozzle velocity is directly proportional to the axial overlap. A higher nozzle velocity favors improved re-

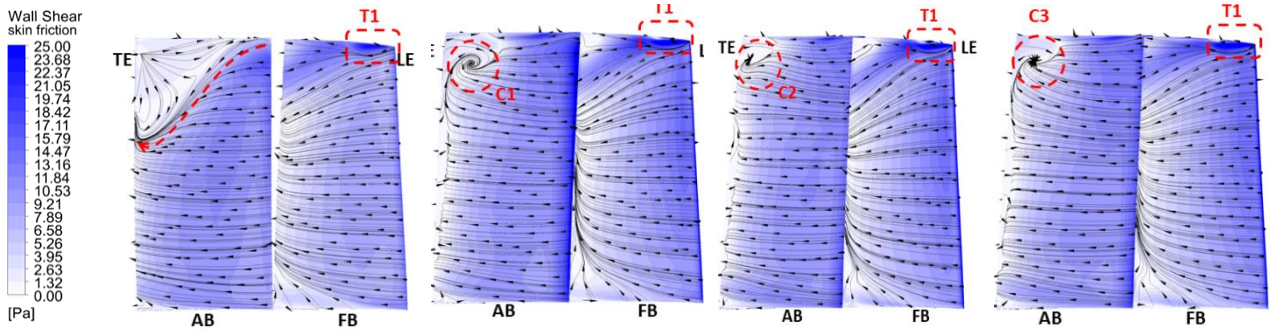

(a) -5 % AO (b) 0 % AO (c) 5% AO (d) 3% AO

Fig. 5 Suction surface streamlines on rotor blades for different AO

energization of the suction surface boundary layer of the aft blade.

6. ROTOR TIP PROFILE MODIFICATION

As the tandem configuration is being implemented for the rotor, running clearances between tip and casing demand a suitable tip shape of both the rotor blades. The cylindrical tip profiles for individual blades results in two peaks and valleys in the rotor tip due to presence of both blades. Both fore and aft blades are projected on two different cylindrical surfaces which results into surface discontinuity at the mid of effective chord.

Authors found this as one of the major design aspects and it was explored in detail. The common cylindrical tip profile for both the blades results in a uniform tip gap between tip and casing considering tandem rotor blades as a single blade. The tip profile of both fore and aft blades are projected onto a common cylindrical surface. Considering mechanical constrains and available manufacturing tolerances, a tip clearance of 3% (of blade span) was provided as representative of typical values for present low-speed experimental facilities.

7. EFFECT OF CHANGE IN AXIAL OVERLAP

The change of axial overlap has a first order influence on overall flow features as well as detailed and minute phenomena of tip clearance flow and passage vortex structure. This section discusses the effect of axial overlap on both global and local flow structures.

7.1. Surface Flow Feature

Initial insights regarding the overall flow physics can be obtained by the suction surface skin friction contours and surface streamlines as shown for all the AO variation (Fig. 5). It can be observed that qualitative behavior of tip clearance vortex for fore blade is unchanged for all the AO variations (Fig. 5a, b, c) region T1]. Thus, fore blade behaves like a conventional compressor blade. It is more interesting to observed that fore blade is unaffected from the relative axial location of the aft blade in terms of tip clearance vortex location. For the base rotor with 0% AO the suction surface boundary layer on aft blade separates at the TE with a re-circulatory pocket formed at 85% span (Fig. 5b region C1). While considering a negative overlap of -5% the migratory boundary layer is observed to have a downward draft and separates at about 70% of the span. The strength of re-circulation has reduced due to reduction in blade loading itself (Fig. 5a). Interestingly the boundary layer remains fully attached below 70% span for both fore and aft blade in comparison to the base rotor case. It is to be noted that both maximum negative and positive axial overlaps are actually realized at the tip region.

The tandem arrangement limits the downward draft to 70% span for -5% AO case. The accelerated nozzle flow from the tandem interface (tandem nozzle) actually sustains an attached surface boundary layer. The tandem nozzle flow becomes weak in higher span region for -5% AO resulting in stall due to higher loading. For a positive overlap of +5% the entire flow field seems different. A uniform suction surface boundary layer profile can be seen up to 90% span (Fig. 5c) for the aft blade. But at the same time the re-circulatory region reappears at approximately the same span location (as observed for 0% AO) but it has reduced intensity and circumferential extent (Fig. 5c) region C2]. In line to 5% AO, for 3% AO the flow field on suction surface of aft blade is found to be improved. It also has a recirculatory region at the same span location with almost the same circumferential extent.

7.2. Tip Clearance Flow

The discussion of stage design methodology is incomplete without emphasizing on tip clearance flow physics as it contributes as a primary source of loss for the rotor. The unmanaged tip clearance flow can interfere severely with main flow which can deteriorate the performance to a significant level. Smith (1975) has investigated the adverse effect of large tip clearance on stability and efficiency of axial flow compressors in detail. The passage flow blockage strongly depended upon the tip clearance flow due to increase in displacement thickness across the blade rows with high tip clearance. As per Koch (1981) the tip clearance flows have a first order negative impact on the pressure rise capability of a blade row. According to the study by Wisler (1985), the tip clearance and end wall flows constitute more than half of the secondary losses in axial flow compressors. Storer and Cumpsty (1991) acknowledge the tip clearance flow in principle as a low loss core bounded on the top and bottom

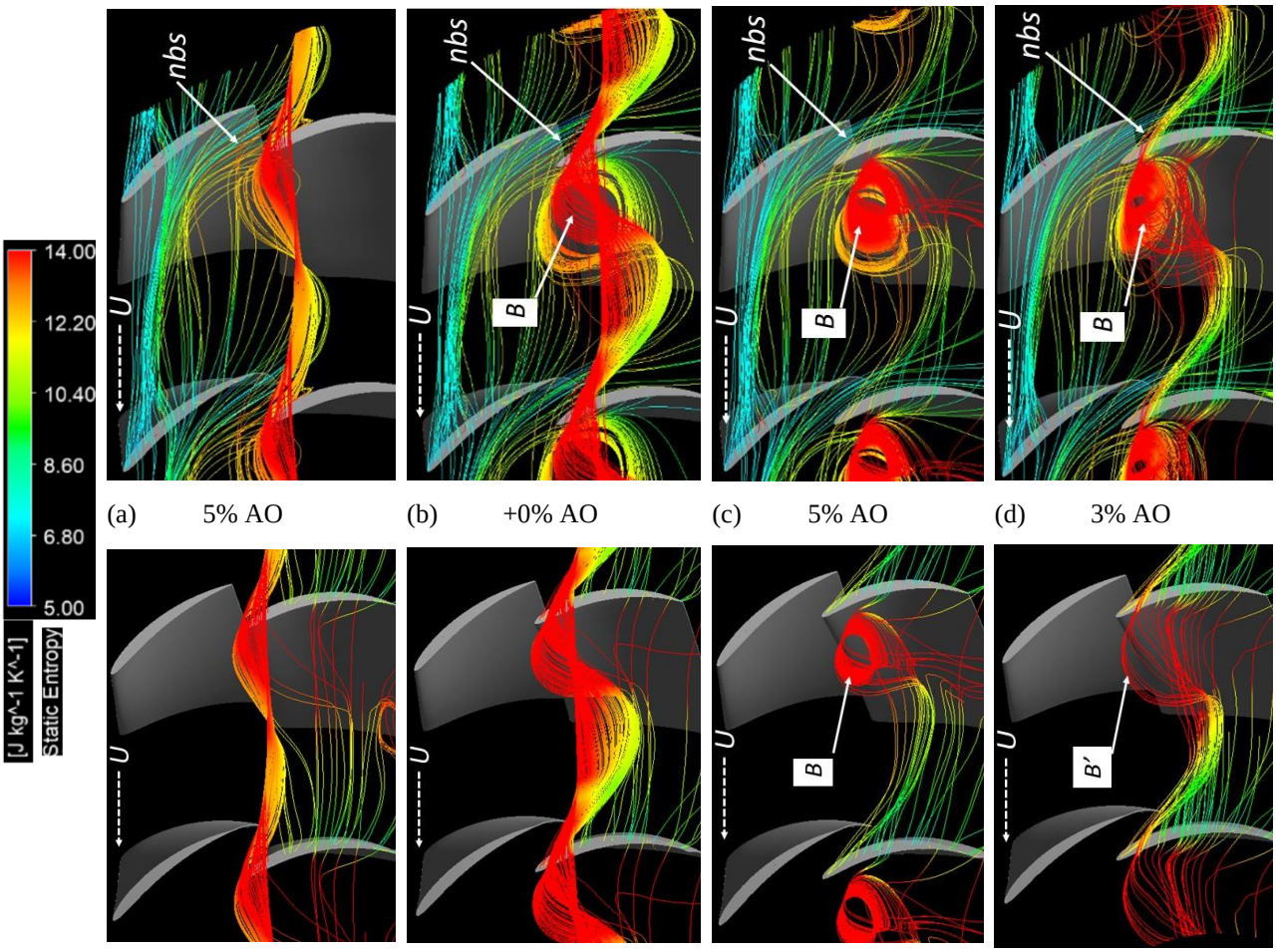

Fig. 6 Blade to blade clearance flow

by a free shear layer. Mixing of the clearance flow with core flow is responsible for the losses while negligible loss of momentum was observed in the gap region itself.

The various loss sources in turbomachines have been described in detail in the study by Denton (1993). The mechanism of tip clearance loss and generation of entropy is attributed to mixing of tip clearance flow with main stream flow. The author also proposed a mixing model for the same. The role of tip clearance flow in the growth of blockage is quantified by Khalid et al. (1999). The authors proposed a methodology to quantify the flow blockage with change in parameters to within 10% of design value. Horlock (2018) further reviewed the quantification of end wall flow blockage in a comparative study. The validity of mixing hypothesis by Denton (1993) was revisited in the detailed study by Sakulkaew et al. (2013). The authors concluded that high tip clearance leads to shift in the loading towards the aft side thus delaying the clearance formation and complete loss potential of clearance flow is not realized. It is suggested that the overall losses are a compromise between viscous and mixing losses in the tip gap region based on which an optimum design criterion is derived. In the case of a conventional rotor, the low momentum fluid leaves the flow passage towards the stator (Tiralap et al. 2017).

The tip clearance flow structure for tandem rotor is entirely different and more complex than a conventional rotor due to presence of two blades. The blade-to-blade clearance flow has been plotted separately for both fore and aft blade for better understanding as shown in Fig. 6**.** It can be observed clearly that clearance flow from the fore blade is split primarily into two parts-

1. As conventional tip clearance flow from pressure surface to suction surface due to differential pressure.
2. Movement of tip clearance flow from the nozzle gap formed due to tandem arrangement.

It is interesting to observe that only a small fraction of tip clearance flow from the fore blade contributes as double clearance flow into the adjacent blade passage. Majority of the tip clearance flow is observed to be sucked in by the tandem nozzle gap before mixing with the main flow in the adjacent blade row. This has been designated as *tandem nozzle by-passed tip clearance stream (nbs)* as it emerges in the adjacent passage via nozzle gap. The nozzle by-passed clearance flow component has a greater impact on irreversible mixing. For positive overlaps (Fig. 6 b, c, d) the bypassed nozzle stream interacts with endwall flow to form a region of low momentum bubble characterized by high entropy region – region B. It is difficult to identify and predict the individual contribution

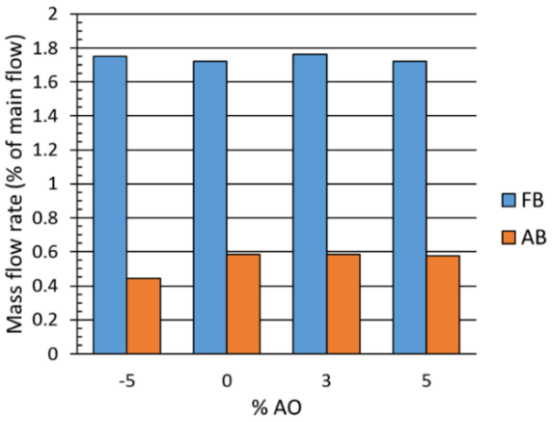

Fig. 7 Mass flux through the tip gap

of primary nozzle flow and by-passed clearance flow in overall mixing and formation of loss region. At the same time the blade-to-blade clearance flow pattern for aft blade (Fig. 6 e-h) is observed to exhibit peculiar behavior in between blade passages. The clearance flow leaves the blade suction surface with dominant streamwise velocity component but changes the trajectory towards the tandem nozzle gap region and again mixes with fore blade clearance flow structure. This results in a very complex flow structure near upper span of the rotor blade specifically near the aft blade. This is characterized by high entropy region in the mid of the blade passage. For the aft blade, the flow field consists of mixing of (a) flow coming out from the nozzle gap and (b) its own tip clearance flow along with wall boundary layer. This results in a very peculiar flow field and as per the knowledge of authors no such flow structure has been reported in open literature. The emphasis on tip flow structure with change of AO is important as highly loaded compressor stages are sensitive to instabilities during off-design operating conditions. The qualitative difference between the aft blade leakage flow for +5% and +3% AO is worth mentioning. The high loading and increased nozzle action (due to high AO) results in more strong mixing of clearance flow with endwall flow resulting in larger area of high entropy fluid (Fig. 6 c) -region B). The case with +3% AO results in gradual mixing of clearance and endwall streams (Fig. 6 d) –region B'). It is tempting to analyze the tip clearance flow through the rotor quantitatively for appreciating the flow mechanics responsible for flow stability and stall. Figure 7 shows the quantity of tip clearance flow through both the blades as a percentage of main flow. As the axial overlap changes from +5% to -5%, the clearance flow through the fore blade increases by mere 1.75% but at the same time the clearance flow through the aft blade decreases substantially. Decreasing the AO results in moving the aft blade away from the TE of the fore blade which decreases the blade loading primarily on the aft blade. In fact, the aft blade has a stall near the tip region (Singh & Mistry, 2019) for negative overlap. This justifies the decrease in tip clearance flux which is governed by this aerodynamic loading. The decreased AO also decreases the loading on fore blade (as per the potential flow theory). Thus the clearance flow through fore blade should also decrease as a consequence. An increase in clearance flow flux is counter-intuitive. One of the effects of the tandem nozzle is to have a suction effect immediately at the TE of the fore blade. The reduction in suction from the tandem nozzle region due to poor nozzle flow is attributed to increased clearance flow through the fore blade. The nozzle stream has both streamwise and cross-stream component and latter results in higher mixing losses with main flow. The case with 3% AO turned out to be a trade-off between sustained suction surface boundary layer and acceptable losses (Singh & Mistry, 2019). The current study contemplates on a different aspect of flow structure in following section and justifies the selection of 3% AO. More insights into the tip clearance flow physics can be gained by analyzing the clearance flow-main flow interface location for the rotor. The interface location is set by momentum balance between the incoming main flow (higher streamwise momentum) and low momentum tip clearance flow (Duc Vo et al., 2008). The entropy per unit mass at 97% span has been plotted to identify the probable location of this interface plane. The clearance flows have higher entropy in comparison to mainstream flows resulting in sharp gradient of entropy at the interface location. At the limit of steady flow simulation accuracy, this interface plane lines up with the blade LE. It is

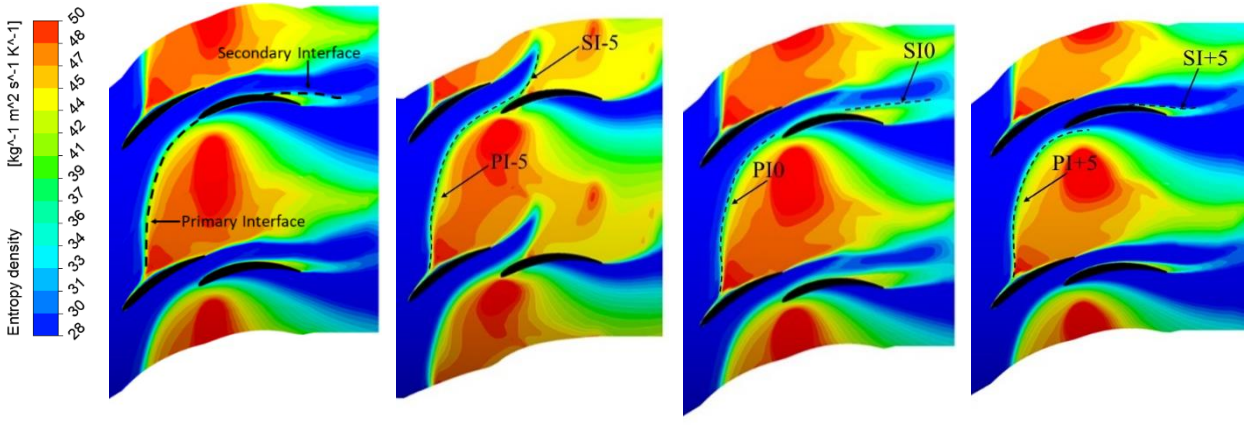

(a) Design Point **(b) -5% AO** **(c) 0% AO** **(d) 5% AO**

Fig. 2 Clearance flow-mean flow interface location

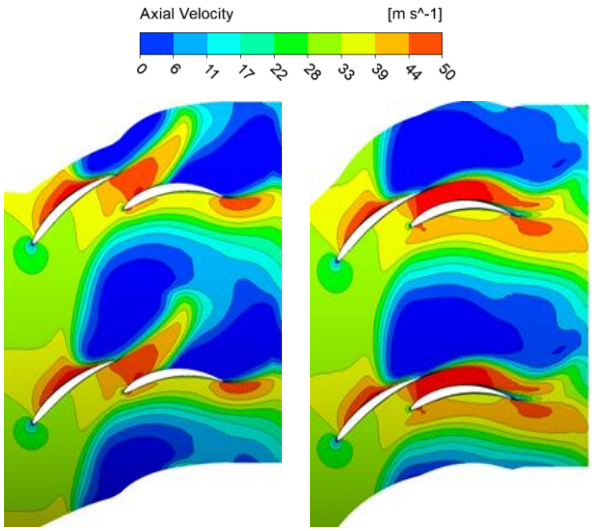

(a) -5% AO (b) +5% AO

Fig. 9 Axial velocity contours at 96% Span

interesting to observe two interface locations (based on entropy gradients) instead of one as described in the relevant literature for conventional rotors.

The interface between passage flow and fore blade clearance flow is termed 'primary interface' and another one emerging through the nozzle as 'secondary interface' as depicted in Fig. 8(a). The location and extent of secondary interface is primarily a result of momentum balance between the aft blade clearance flow, tandem nozzle flow and mainstream flow. The effect of change of axial overlap can be observed primarily on the secondary interface as it shifts closer to the suction surface of aft blade with increasing AO. This indicates higher momentum of nozzle flow. In the tip region, the tandem bladed rotor has an additional mechanism of loss other than tip clearance flow. It can be observed from the axial velocity contour at 96% span that at -5% AO, the aft blade has a premature stall (around 40% of chord) while fore blade has a TE stall (Fig. 9a).

It is interesting to observe that interface location aligns in close proximity with low momentum stalled flow for the aft blade (for all configurations) but lies upstream of fore blade stall. This is because entropy gradient is dominated by mixing of high momentum incoming flow and tip clearance for fore blade. The statement is also supported by comparing the quantity of clearance flow from both blades. The mass flow through the tip gap for aft blade is about 68% lesser than that from the fore blade. For the base case (Fig. 8c) (0% AO) the primary interface begins from about 30% chord of fore blade and terminates at LE of aft blade (PI0). As axial overlap changes to -5%, the location of primary interface relative to fore blade remains almost same (PI-5). The secondary interface in this case is not fully developed due to weak tandem nozzle momentum (SI-5). As observed from Fig.7 the mass flux through the fore blade tip gap increases at -5% AO. The local blade loading decreases with reduced AO but the slight increase in total clearance flow is speculated to come from reduced suction of tandem nozzle. In the context described earlier, the bypass clearance flow reduces and this contributes to increases flow from the fore blade tip gap. The authors have used the word 'speculated' because it is uncertain to determine the quantity of bypassed clearance flow. As the axial overlap increases to +5%, the primary interface originates from the same relative location of fore blade but continues entirely inside the blade passage (Fig. 8(d) (PI+5)). This is primarily a consequence of higher local axial velocity due to enhanced tandem nozzle effect and decrease in cross stream component of clearance flow. The secondary interface for +5% AO is aligned with the suction surface of aft blade indicating higher tandem nozzle streamwise momentum (SI+5). The unique interface characteristics of tandem rotor motivates to dig in the details of phenomena in the blade passage and also at the exit of rotor. A detailed in-passage flow field characteristic for wake and vortex structure is described in the next section.

7.3. Evolving Wake Structure

The presence of two highly loaded blades results in dual wake structure formation at the rotor exit. The resulting wake structure at the rotor exit is a consequence of interaction of evolving wakes with the shroud boundary layer and tandem nozzle flow through the blade passage. The twin wake system from rotor is unique flow feature of tandem configuration and requires more attention during design stage for the rotor as well as for the downstream stator. The above-mentioned flow variables can be best understood by following the entropy growth in the blade passage (Fig. 10). As a consequence of higher aerodynamic load split a well-defined sharp wake is seen to exist at the TE of fore blade for all configurations. The result of interaction of tip-clearance flow from fore blade and endwall region is also observed as region of higher entropy with increased gradient towards the end wall. It can be observed that entropy generation in the endwall region increases with positive overlap. This is attributed due to increase in fore blade loading and thus stronger tip clearance flow. This complex system of irreversibility moves downstream with increase in both spanwise and circumferential extent. At 50% chord of aft blade the contributions from the aft blade along with fore blade are clearly evident. For -5% AO the emerging entropy growth from the aft blade is actually a primary consequence of blade stall rather than due to clearance flow. The negative overlap increases the tandem nozzle gap area without any considerable nozzle effect and this lets the higher mass flow to pass through the flow passage (Singh & Mistry, 2019) which mixes with the fore blade wake and then diffuses the flow a bit as in comparison to 0 and +5% AOs (B1,B2 and B3 in Fig. 10). The flow structure for 0% and 5% AO has no qualitative changes at this particular axial location. But at the TE of aft blade, the contribution of aft blade loading is clearly evident with formation of aft blade wake coming along with endwall loss. It can be observed that tip clearance flow structure from the aft blade merges with the tandem nozzle flow and the identification of individual contribution of losses is somewhat ambiguous at this stage. Interestingly at the rotor exit, both the wakes and endwall irreversibility haven't merged and can be distinguished. This results in non-uniform velocity flow

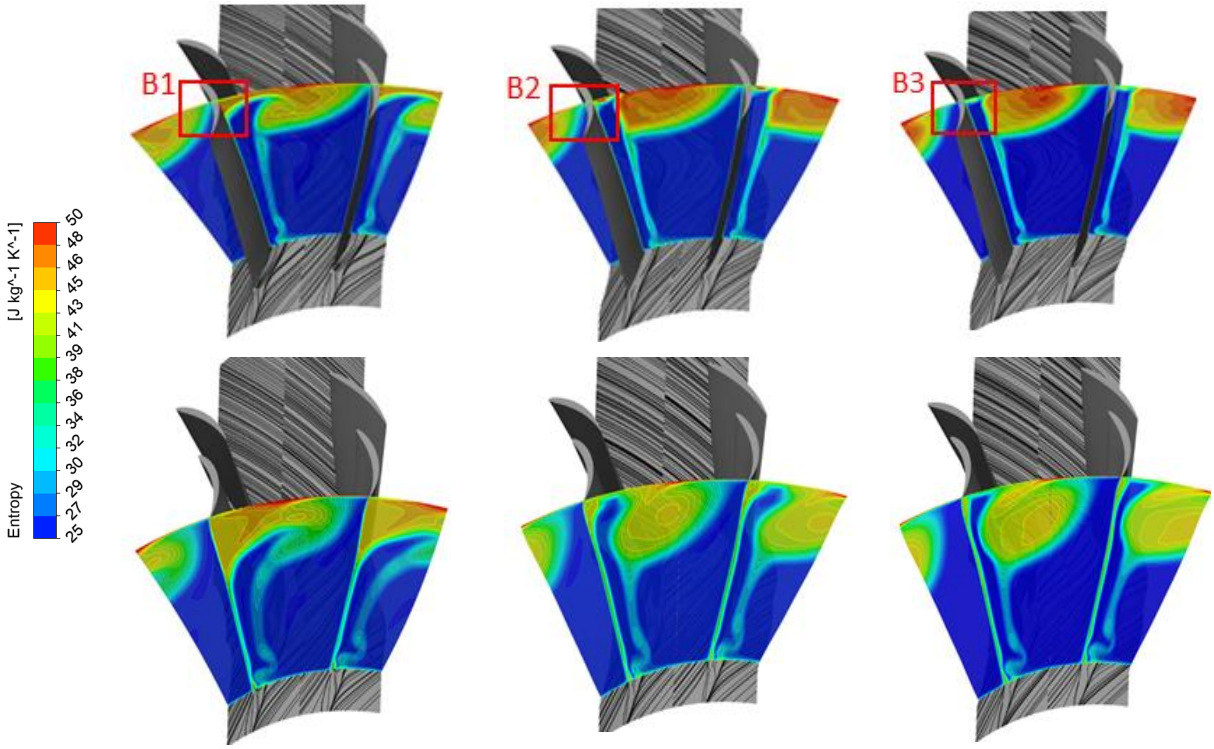

(a) -5% AO (b) 0 % AO (c) +5% AO

Fig. 10 Entropy growth within the passage

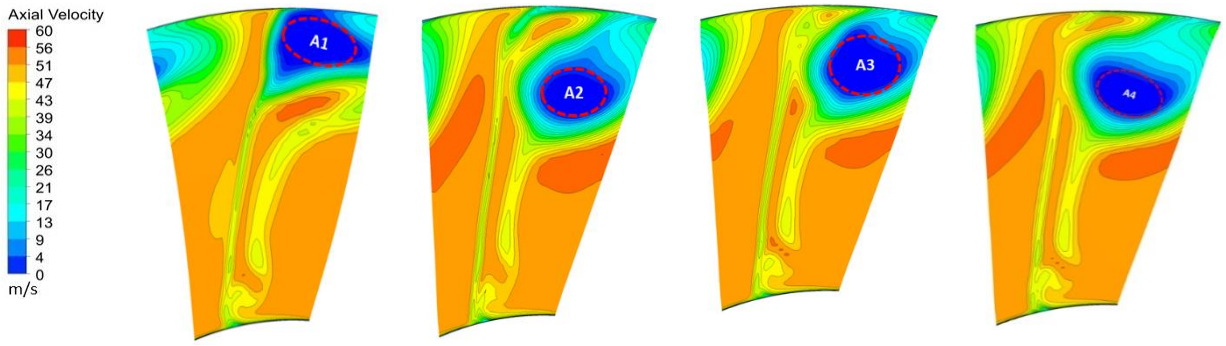

(a) -5% AO (b) 0% AO (c) +5% AO (d) 3% AO

Fig. 11 Axial velocity field at rotor exit

field at the rotor exit plane. This can be attested from Fig. 11 which shows the distribution of axial velocity at the exit plane. The low momentum bubble at the rotor exit changes its spanwise as well as circumferential extent with the change of axial overlap (region A). For -5% AO it seems to be more near the end wall region and interestingly merged with the aft blade wake. This is in agreement to the TE stall of the aft blade itself as discussed earlier. The momentum bubble gets detached from the end wall as well from the aft blade wake for 0% and 3%. This is due to higher tandem nozzle velocity resulting in velocity gain between aft blade wake and low momentum fluid region.

7.4. Blade Passage Vortex

The interaction of clearance flow and endwall boundary layer results in formation of vortex structure in the blade passage. It is the strength and structure of the vortex at the rotor exit which determines the aerodynamic complexities of the downstream stator. The computational results enable several ways of vortex visualizations. A brief discussion of the advantages and limitations of available methods can be reviewed in the study by Jiang et al. (2005). The vortex structure in the current study is discussed in terms of 'normalized helicity' as proposed by Inoue et al. (Inoue et al., 1998; Inoue & Furukawa, 2002) in the detailed discussion of tip clearance vortex and breakdown. The normalized helicity is defined as

$$\xi_s = \frac{\vec{\xi} \cdot \vec{V}}{|\vec{\xi}||\vec{V}|} \tag{5}$$

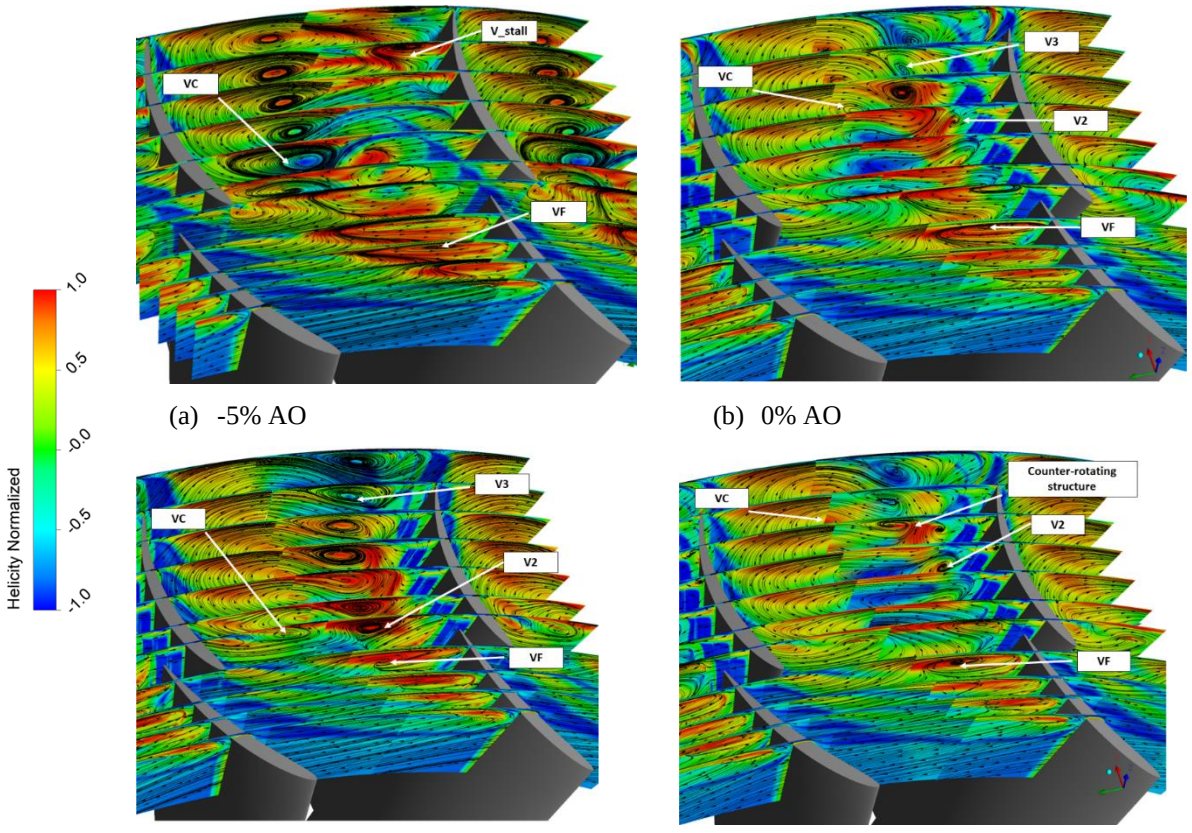

(a) -5% AO (b) 0% AO

(c) +5% (d) 3% AO

Fig. 12 Blade passage vortex structure

Mathematically it represents the cosine of angle between the absolute vorticity and velocity vector. Thus, the magnitude of normalized helicity tends to unity in the vortex core region. The range of normalized helicity is ±1 and the sign indicates the direction of swirl of vortex relative to streamwise velocity component. The vortex core passes through the maximum value of normalized helicity and streamlines passing through the immediate vicinity of maxima are twisted (Levy et al., 1990). Figure 12 shows the distribution of normalized helicity along with surface streamlines at various streamwise sections for different AOs. The circulatory streamline patterns arecoincident with points of maximum helicity at both positive and negative values. Three vortex structures are evident in all the cases – (a) tip clearance vortex of fore blade, (b) vortex due to blade stall and (c) a counter vortex structure. It is imperative to identify the vortex structure in reference to 0% AO (Fig. 12 b). The vortex due to tip clearance flow from the fore blade is clearly evident and identified as 'VF'. The primary effect of tandem nozzle flow is to reduce the intensity of 'VF' as seen from the helicity contour at the TE of fore blade. As observed from the streamline distribution, the tip-clearance flow from the aft blade combines with nozzle flow. This complex interaction results in formation of a second vortex structure 'V2'. The intensity of 'V2' increases locally till 80% chord of aft blade and decreases afterwards. The quick gain of intensity for 'V2' results in a counter-vortex structure designated as 'VC'. The exit plane of rotor contains two differentiable vortex structures due to the discussed interactions. The change of helicity sign indicates a possible breakdown of vortex structure in blade passage (V3) and a dedicated study is required in order to identify the exact reason of breakdown. The primary intent of the current study is to justify the selection of AO in the light of resulting exit flow vortex structure for facilitating the design of the stator. The vortex structure for +5% AO (Fig. 12 c) is similar but quantitatively different. As discussed in tandem nozzle mass flow characteristics the case with +5% AO has highest velocity through the tandem nozzle (Fig. 4c). This results in early formation of 'V2' (in comparison to case with 0% AO) with increased intensity. Coincidentally the counter vortex VC also appears early as shown. The vortex structure 'V2' weakens a bit as it proceeds towards the TE and finally exits the blade passage as 'V3'. It is important to notice that exit vortex structure for +5% AO configuration is more intense in comparison to 0% case. The vortex structure for -5% AO is quite different due to severe stall of the aft blade in the tip region (Fig. 12a). The resulting vortex is identified as 'V_stall'. The flow passage is dominated by the counter-vortex (VC) which lies in the mid-blade passage. The finalized case with +3% AO shows a distinct vortex distribution resulting in less severe flow structure at the exit. The vortex structure 'V2' is seen to split into two weak counter-vortices before exiting the blade passage. As discussed in the study (Singh & Mistry, 2019) the streamwise component of velocity through the tandem nozzle is highest for +3% AO and cross-stream component is highest for +5% AO. The high cross-stream component of tandem nozzle flow results in severe strength of V2 (due to increased shear flow). The

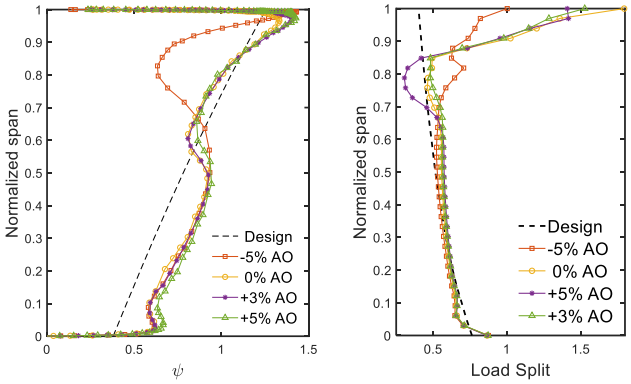

(a) Pressure rise coeff. (b) Load Split

Fig. 13 Spanwise distribution of at rotor exit

streamwise component results in less intense V2 structure which further dissociates into two weak counter-vortices. It is now clear that the AO is a sensitive parameter in the sense of design as it has a major impact on exit flow field. For the present design +3% AO was selected in order to reduce the flow three dimensionality which will be incident on the stator. The changes in performance of rotor alone in terms of spanwise pressure rise are insignificant for +3% AO when compared with +5% AO (Fig. 13a). The consideration of downstream stator requires more careful selection of geometrical parameters for the tandem bladed rotor.

7.5. Spanwise Loading and Load Split

As part of design strategy the rotor has been designed with an increasing spanwise pressure rise coefficient to maximize the benefits of tandem nozzle effect (Fig. 13a)-dashed black curve]. For different axial overlaps, the numerically calculated ψ variation follows the targeted design trend but has a larger magnitude throughout the span except 60-80% region. The aerodynamic leverage gained due to tandem nozzle effect results in a considerable higher loading than expected as the former was not considered during the initial design. Nevertheless, the configuration with -5% AO is severely compromised after 70% span due to aforementioned stall.

All other cases including 0% AO are in positive agreement with desired loading profile. The slight depression between 60%-70% span is a consequence of three-dimensional mixing losses associated with endwall boundary layer and tip clearance flow. It is a common feature for all the configurations. Interestingly the low pressure profile is at a higher span for the case with -5% AO. The decrease of loading on aft blade in the higher span regions can be attributed for this behavior. Decreased loading results in very weak tip clearance flow from the aft blade itself. The losses are primary a consequence of blade stall which is localized nearer to shroud.

There is considerable overturning of the flow over 70% span due to very low deviation angles. The empirical relationship for deviation angle is based on conventional cascade data. The presence of tandem nozzle jet in upper span favors turning of flow from both the fore and the aft blade TE thus permitting higher turning than expected. It is difficult to ascertain the individual contributions of blades in achieving the desired pressure rise due to presence of blade overlap and high velocity jet issuing from the tandem nozzle. However, a computationally calculated load split based on diffusion factor [Eq. 4] can be compared with desired load split curve [dotted black curve in Fig. 13(b)]. The desired load split curve indicates that loading on aft blade increases from hub to tip. As mentioned earlier both the blades are differently loaded and the load split is given by Eq. (4). It is interesting to observe that though overall loading surpasses the design expectation but load split is in close agreement with proposed ratio till 75% span. The configurations with -5% and +5% AO lie on different sides of design curve after 75% span. The undershoot by -5% AO case basically indicates decrease of loading on aft blade due to stall. This trend continues till tip region where loading on aft blades decreases significantly. On the other side the overshoot by +5% AO case is due to higher aft blade loading sustained by tandem nozzle flow. As axial overlap increases the loading on the aft blade further increases due to tandem nozzle action as a benefit. Hence the load split surpasses the design value in higher spans. The curve departs away from the desired value after 90% span due to three-dimensionalities prohibiting loading on aft blade in this region. The mixing of fore-blade wake, tip clearance and endwall flow have detrimental impact on the local loading characteristic of aft blade. The case with 0% and 3% AO are in close agreement with loading distribution till maximum extent of span.

8. DESIGN ASPECTS FOR THE STATOR

The three dimensional flow field associated with tandem bladed rotor are readily carried on to the stator. For the present stage design, the non-uniform velocity profile at the rotor exit possesses very challenging inflow conditions for the stator. While designs in open literature suggest tandem rotor-tandem stator arrangement (Eshraghi et al., 2014; Boroomand et al., 2016) the dual tandem configuration in single stage shall invite extreme three-dimensionalities as a legacy of individual tandem configurations. The objective of the design procedure is to accommodate a single bladed stator with axial exit. This results into considerably higher fluid deflection through the stator. The overall design parameters of stator are summarized in Table 2. The higher fluid deflections facilitated by the tandem arrangement have evolved into very challenging performance constrain for the stator. The diffusion factors are of the order of 0.7-0.8 which surpass the conventional limit for low-speed stators. The detailed strategy for designing the stator has been described in the dedicated study (Singh & Mistry, 2020).

This section dissects the flow physics which gives more clarity and understanding while designing such stage configuration. The absence of any guidelines for approaching such a design led to start the design process from the fundamental understanding based on available

Table 2 Design parameters for stator

Overall parameters of rotor			
Parameters	Hub	Mean	Tip
σ_T	2.24	1.50	1.12
DF_T	0.34	0.58	0.73
Design parameters for base stator			
Parameters	Hub	Mean	Tip
$\Delta\alpha_s$	53.25	59.72	62.58
DF_s	0.53	0.70	0.81

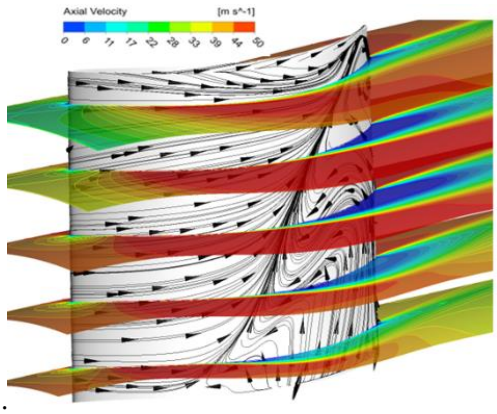

(a) Spanwise axial velocity

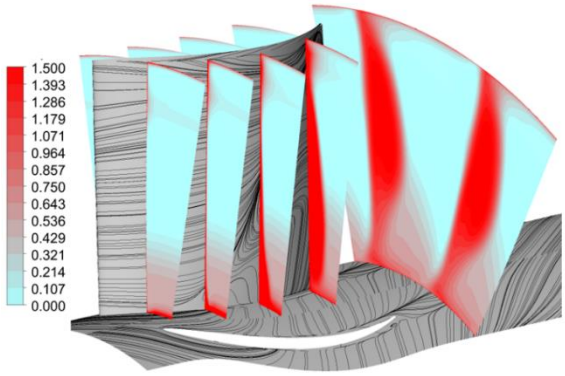

(b) Total pressure loss

Fig. 14 Spanwise axial velocity profile and total pressure loss for base stator

open-source literature. In order to address very high flow turning angle, a circular arc cambered stator in combination with C4 thickness distribution was used as the base case. In order to manage the flow through the stator, it is obligatory to describe the flow physics for the base stator and identify the flow complexity and the associated challenges.

The spanwise axial velocity contour indicates unacceptable flow separations throughout the span towards the trailing edge of the stator blade (Fig. 14 a). The stator blade stall initiates from 30% chord (at hub) and proceeds almost linearly towards the trailing edge at higher span locations. The velocity contours line up with the suction surface separation line as shown in Fig. 14 and clearly indicate the flow separation on the suction surface of the stator blade. This flow separation manifests as evolving loss of total pressure throughout the passage as shown in Fig. 14(b). The total pressure loss coefficient contours at different streamwise locations give a clear idea of the origin of losses with the resulting loss region at the exit of the stage. The exit plane has considerable total pressure deficit and flow separation throughout the span. The detailed flow field observation on stator suction surface clearly shows the higher total pressure loss throughout the span. The separation line on suction surface also reveals the delayed acceleration especially in the mid-span region. It is to be noted here that the flow three-dimensionality along the span is not only because of local flow separation at particular section but it is combination of different flow features such as (a) twin wakes coming out from rotor, (b) flow incidence along spanwise direction and (c) higher turning of flow throughout the span. A peculiarity of the separation profile can be readily observed as majority of the separation is centered around core span regions as opposed to endwall regions. This is a consequence of rotor exit flow non-uniformity which is around 80% span at the rotor exit plane. This blockage bubble has a downward draft and thus influences the stator in the core regions. The stator hub is relieved due to low loading of the rotor in the hub region. Different design approaches based on detailed flow field were explored and are discussed in following sections.

8.1. DCA Cambered Stator

One of the strategies in approaching such a design is to limit the flow diffusion in the stator passage by implementing custom tailored airfoil shapes. The adoption of circular arc camberline for such higher turning led to mid-loaded flow configuration. After iterating through a number of other camberline shapes e.g., exponential, parabolic, polynomial etc. it was decided to implement the double circular arc (DCA) camberline owing to its flexibility of aerodynamic loading control. The DCA camberline has wide implementations in the design of custom-tailored airfoil shapes in the past for desired flow control along the chord. The conventional circular arc camberline has equal (and opposite) slopes at the LE and TE resulting in maximum camber at 50% chord. The DCA camberline facilitates different LE and TE metal angles with controlled turning distribution along the chord. Basically, it consists of two circular arcs which are blended at any desired chord location giving more flexibility to manage the flow. The generation of DCA camberline requires four inputs from the user (Fig. 15a) – LE angle (α_{LE}), TE angle (α_{TE}), blend angle (α_b) and blend location (x_b). The LE and TE angles are basically derived from the stage velocity triangles at particular station but the flexibility of selection of blend angle and blend location provides great control to achieve desired flow management. The mathematical procedure of generation of DCA camberline are described in the detailed reports by Frost et al. (Frost et al., 1972; Frost & Wennerstrom, 1973). Figure 15(a) shows the resulting blade shapes by two different DCA camberline shape with same LE, TE angle, and blend angle. It clearly shows that the flow passage area can be changed by changing the blend location. The placement of blend location towards or away from the LE results into a fore loaded and aft loaded blade

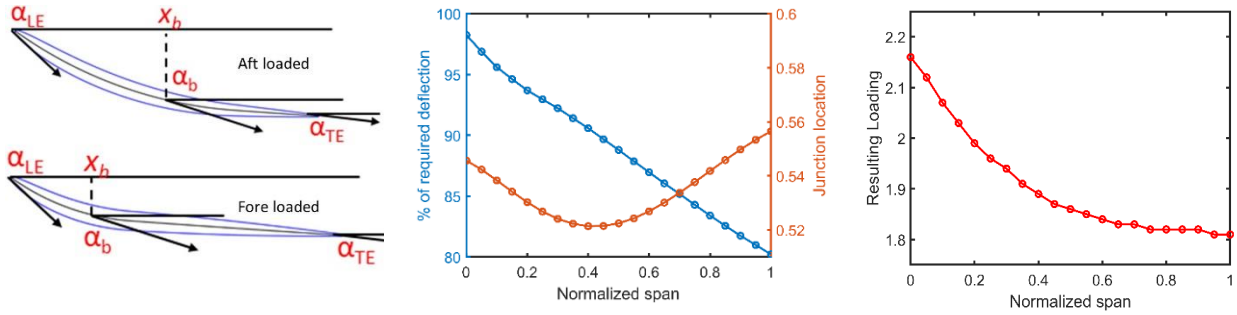

(a) DCA cambered airfoil shapes (b) Spanwise turning and Junction location (c) Loading factor

Fig. 15 DCA camberline variations

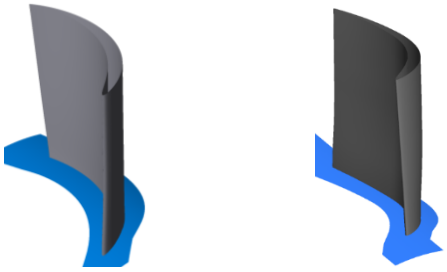

(a) Base stator (b) DCA cambered stator

Fig. 16 3D shape of base and DCA cambered stator

shape (Fig. 15 a) respectively. The resulting blade passage shape manages the flow within the passage to meet the expected flow diffusion rates. The flow deviation angle is calculated based on empirical results derived from the extensive cascade data. The cascade data are available for more standard circular arc camberline, parabolic camberline and NACA series. As there can be practically infinite shapes for given LE and TE angles resulting in different camberline shapes, there is some degree of ambiguity in the estimation of deviation angle for the DCA cambered airfoil. To be on the conservative side the deviation angle calculated for circular arc camberline have been increased by 20% to rule out any chances of flow under-turning. The definition of DCA shape for given camber angle depends on two independently controlled parameters – blend angle and blend location.

In order to include the effect of these parameters, it is proposed to club these two into *shape loading factor* defined by

$$loading\ factor = \frac{\Delta\alpha_b}{(1 - x_b) \times 100} \tag{6}$$

Where $\Delta\alpha_b = \frac{\alpha_{LE} - \alpha_b}{\alpha_{LE} - \alpha_{TE}} \times 100$; represents the percent of required total turning executed by the blend location. *Shape loading factor* provides an estimate of loading distribution from the LE. The definition is solely based on geometric shape and disregards viscous effects and three-dimensional flow interactions along the span. Figure 15(b) compiles the spanwise variation of turning and blend location used in the present design. The shown variations are arrived at with a number of iterations and flow field analyses. A strategy based on prescribing higher percentage of required total deflection near the hub region and its magnitude reducing linearly across the span (Fig.1 5 b) -blue] was implemented finally. The spanwise blend location starts from 54.5% of chord at hub and reduces to around 52% at mid-span and again increase to 56% at tip region resulting in a loading factor distribution as shown in Fig.15(c). The slight kink in the loading curve at 90% span is a consequence of mild corrections in parameters for ensuring expected aerodynamic match which is discussed in detail in the following sub-sections. The thickness distribution of C4 airfoil was wrapped around the resulting camberline distribution as shown in Fig. 16.

The observation of loading factor reveals fore loaded stator blade shape from hub to tip. The 3D blade shape corresponds with the fore loaded blade shape in comparison with the conventional stator as discussed earlier (Fig. 16). DCA cambered airfoil results in improved flow passage till 70% span in comparison to the base stator design case (Fig. 17a).

It should be noticed that 80%-90% span region experiences severe blade stall. This flow separation is mainly due to extreme forward loading which results into higher blade curvature near the LE. An overall performance improvement can be noticed from the pressure surface limiting streamlines (Fig. 18 a, b). The spanwise migration of boundary layer is more gradual in case of DCA cambered stator in comparison to the conventional. stator. The radial pressure gradient has been controlled to a significant degree especially in the lower to mid-span regions. For the lower half of the blade the change of aerodynamic loading characteristics between circular arc cambered stator and DCA cambered stator can be appreciated by comparing the *Cp* distributions. The fore loading is primarily a consequence of changes in pressure distribution on the pressure side of the airfoil (Fig. 18c). It can be clearly revealed that desired diffusion is achieved by about 40% of chord for DCA cambered airfoil while it continues till TE for conventional circular arc cambered airfoil. The DCA cambered stator exhibits slight acceleration of flow on pressure surface after 40% of chord till TE. This leads to reduce the overall blade loading on the airfoil at particular location but contributes

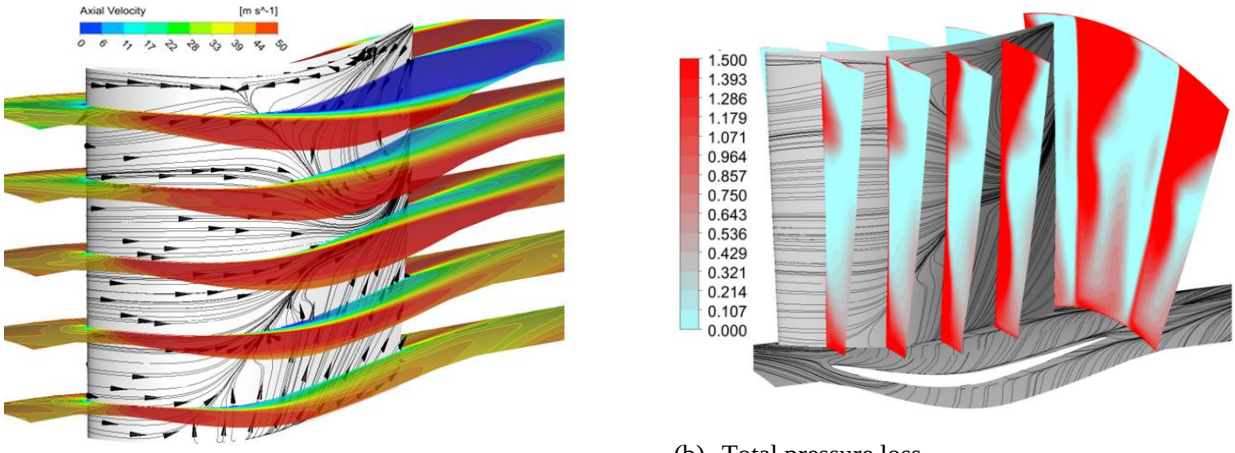

(a) Spanwise axial velocity

(b) Total pressure loss

Fig. 17 Spanwise axial velocity profile and total pressure loss for the DCA cambered stator

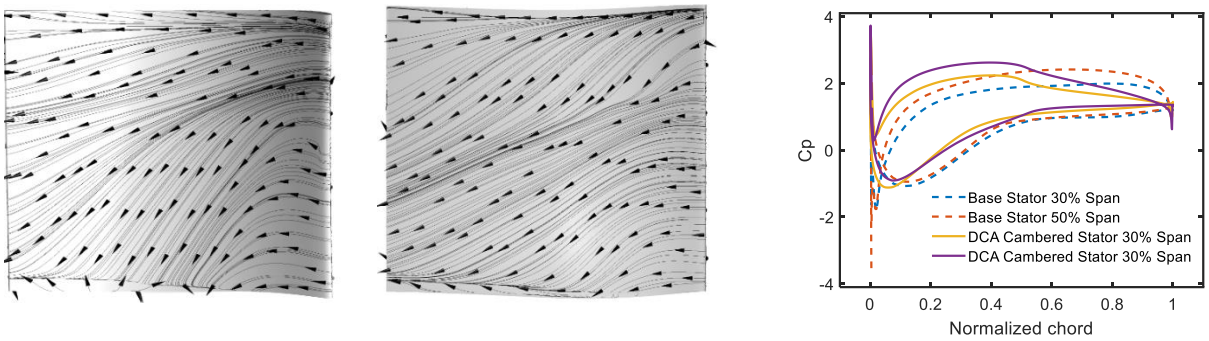

(a) Conventional stator (b) DCA cambered stator (c) Cp distribution for base and DCA cambered stator

Fig. 18 Pressure Surface streamlines for Conventional and DCA cambered stator

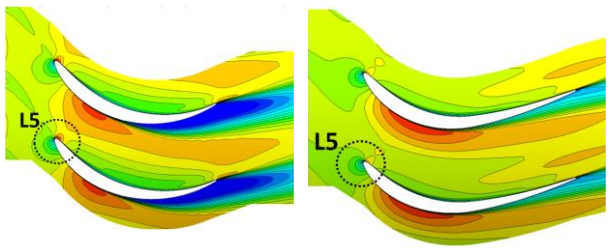

(a) Conventional sator (b) DCA cambered stator

Fig. 19 Axial velocity contour at 50% span for base and DCA cambered stator

positively by letting the flow pass through the passage without severe stall till mid-span region. The detailed flow observation near the LE clearly indicates the different flow behavior. The flow approaches the LE with negative incidence which results into a velocity spike on pressure surface (L5 in Fig. 19. But DCA cambered configuration clearly shows the management of flow near the LE. The flow acceleration is not as high as was observed for the conventional stator which can be observed in Fig. 19(b) and Fig.18(c). The lower span regions are highly benefitted from the fore loading arrangement according to loading factor distribution shown in Fig. 15(c) but at the same time higher span regions are adversely affected. This is one of the reason the loading was gradually shifted towards the TE after 80% span. The rapid change in loading profile from fore side to aft side of the blade is not a feasible solution as it puts limitations of manufacturing aspects due to resulting typical blade shape. The maximum possible corrections have been incorporated assuring feasible changes in three-dimensional shape (the kink in loading curve). By doing so it was found that the location of maximum total pressure loss has been limited to higher span regions (70% span to shroud).

8.2. Endwall Dihedral and Re-Stacking of Stator Blade

The three-dimensional stacking methods provide flexibility in managing the radial pressure gradient which redistributes the blade loading in the spanwise direction. Stators being stationary are open to changes in structural re-configuration as opposed to rotors which have strict constraints due to structural limitations. There are widely accepted diversities in the definitions of 3D stacking lines in the turbomachinery fraternity like *dihedral, bow, sweep* and *skew* (Smith & Yeh, 1963; Gallimore et al., 2002; Vad, 2008) with variants in each category. To address the

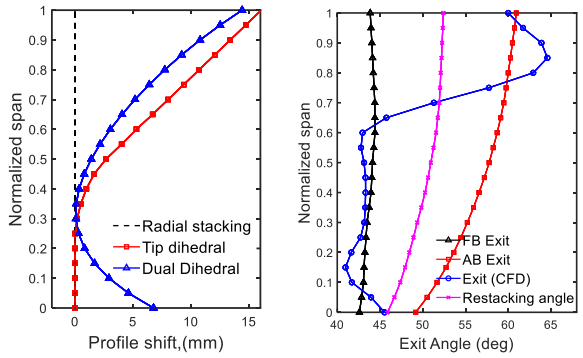

(a) Dihedral profiles (b) Exit angles

Fig. 20 Geometrical parameters of 3D stator

issue of large flow separation along the span, the endwall dihedral was explored for the present design. It is obligatory to clarify the definition of dihedral used in the current study – the displacement of a blade section profile perpendicular to the chord in either direction. The dihedral is called positive if the suction surface makes an obtuse angle with the endwall (which is 90 deg for the radially stacked stator) and vice versa.

Based on detailed flow field study with different design iterations two such profiles are presented here for the discussion. Later on, the dual dihedral was finalized (Fig. 20). The logic behind the selection has been addressed in the dedicated study (Singh & Mistry, 2020). While analyzing the detailed flow field throughout the stage it is evident that design procedure for stator becomes more challenging due to behavior of flow angles at the rotor exit. As discussed earlier, the dual wake and momentum deficit flow coming out from the rotor has great impact on the flow incident on the stator which is not addressed in any literature known to authors. In conventional design approaches, the absolute flow inlet angle for the stator is assumed to be same as absolute flow angle at the rotor exit. Interestingly for the tandem rotor the actual absolute flow angle carries the legacy of both the fore blade and aft blade exit angles. Owing to differences in aerodynamic loading and relative placement of blades (AO), the flow exits with two different wakes and angles coming out of the rotor. The computationally derived rotor exit angle (Fig. 20 b)- blue curve] is plotted with the designed fore and aft blade exit angles. It is interesting to observe that the exit angle is in agreement with fore blade exit angle till about 60% of the span. It then shifts towards the designed aft blade exit angle with some over-turning. It is speculated that effect of fore blade geometry dominates in the exit flow field because of two reasons – higher loading of the fore blade and less axial overlap in the lower span region. The highly twisted flow coming out from the tandem rotor makes whole flow field change at the LE of stator and hence design of stator to meet such requirement becomes difficult. It is not possible to design a stator with such spanwise behavior of LE metal angle. An innovative design strategy is proposed and adopted by considering the metal angle as an average of fore blade and aft blade exit angles (Fig. 20b)- green curve]. This.is to ensures better alignment with the flow

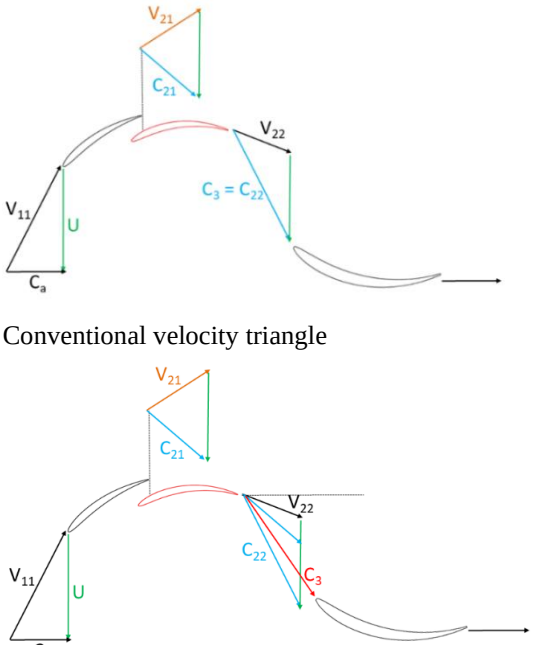

Conventional velocity triangle

(b) Proposed modified velocity triangle

Fig. 21 Velocity triangle at rotor exit

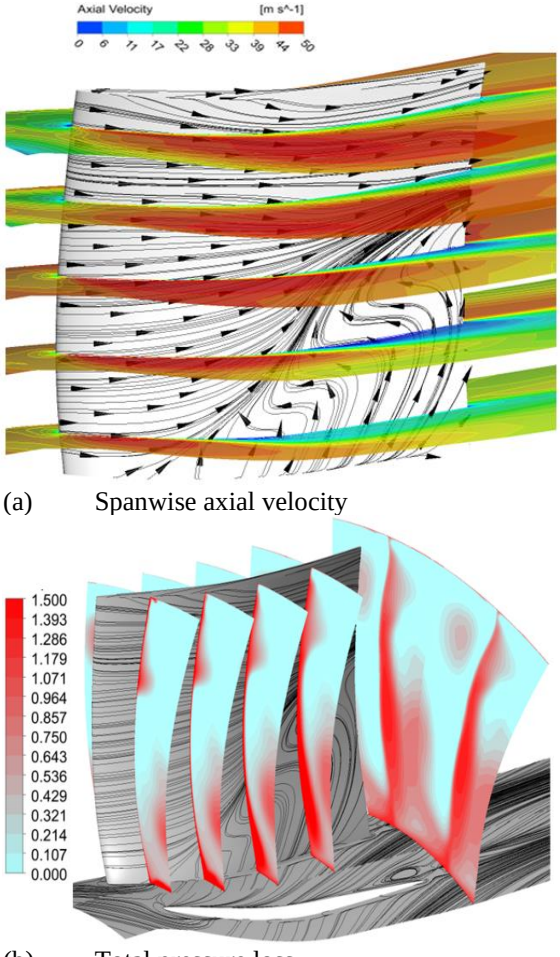

(a) Spanwise axial velocity

(b) Total pressure loss

Fig. 22 Spanwise axial velocity profile and total pressure loss for the 3D stator

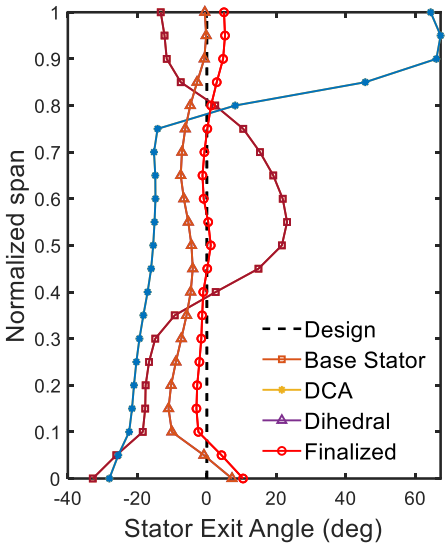

Fig. 23 Stator Exit angle for various configurations

incident on the stator. This can also be demonstrated from the velocity triangles for the stage (Fig. 21a). The conventional design approach mandates stator inlet velocity equal to rotor exit absolute velocity, i.e. $C_3 = C_{22}$. However as discussed there are two effective velocity triangles for the rotor. The direction of absolute inlet velocity has been proposed to be that of average of exit velocities from fore and aft blade as shown. Authors would like to emphasize that it is not a correction of inlet incidence as differences in exit angle are of the order of 12 degrees. The reason for such flow non-uniformity is attributed to the discrete wake structure along with endwall blockage flow coming out from the rotor. The spanwise axial velocity contours and total pressure loss profile (Fig. 22) indicate improvement of flow quality along the span at the exit of the stage compared with conventional and previously used stator design methodology. There are separations at 30% and 50% span due to slight mismatch into the flow angle. An exact LE metal angle match is possible but it may affect the performance during off-design operating conditions and may lead to reduction in overall operating range. Hence no further modification in flow angles is incorporated. The final design has been arrived by iterating through a number of configurations. Since the stage has been designed with a goal of integration within the core compressor stages of an engine, the stage exit flow angle is one of the primary quantitative and qualitative parameter of performance evaluation. Figure 23 compiles the spanwise variation of stage exit angle for various stator designs. As expected, the base stator has considerable over- turning till hub to 30% span. This is followed by considerable under-turning till 70% span which again results in over-turning above 80% span. The endwall effects and mid-span stall (section 8) result in an uneven angle profile at the stage exit. As discussed in section 8.1 on DCA cambered stator a relatively uniform exit angle distribution can be expected till 80% span which shifts to under turned regime afterwards due to stall in the tip region. The extreme under turning can be expected from the velocity and loss contour discussed in reference to Fig. 17. The dual dihedral and finalized design have close tolerance to intended exit angle distribution (black dotted line: Fig. 23). Slight under-turning in the hub and tip region can be observed for the finalized design (red curve) due to deliberately relieved loading in the endwall regions.

9. CONCLUSIONS

Based on the number of systematic design iterations, it is well understood that design efforts need to be centered around the rotor-stator aerodynamic match. The selection of geometrical parameters has a first order influence on overall performance of the stage. The study outlined a sequential design methodology rather than discussing the permutations of all the possibilities. Based on proposed queries in the introduction section and as per the systematic sequence of the study the following conclusions can be drawn -

9.1. Design Aspects of Rotor

- The aero-thermodynamic design of a tandem bladed rotor is governed by three major factors –Load split between the fore and aft rotor blades, spanwise load distribution (Total pressure distribution) and shape of nozzle geometry formed due to tandem blade arrangement.
- Current tandem blade configuration is with target of higher aerodynamic loading of fore blade (around 60%) while aft blade is lightly loaded (40%). The flow incidence variation in fore blade is taken care of to a certain degree by passive flow control offered by the tandem nozzle. The aft blade receives a pre-conditioned flow from the fore blade and hence it has been mildly loaded to accommodate incidence changes during off-design condition. An experimental analysis is under proceeding to attest the load distribution logic.
- The spanwise distribution of aerodynamic loading for both fore and aft rotor blades individually has been strategized with a view to derive the benefits from tandem nozzle effect. This particular stage has been designed with a controlled vortex approach with increased loading at higher span regions to optimally harness the aerodynamic benefits due to tandem nozzle shape.
- The control of tandem nozzle geometry has been achieved by systematically varying the axial overlap. The selection of axial overlap has been strategized to assist the spanwise loading distribution in the best possible way. A linearly varying axial overlap of 0% at hub to 3% at tip performed optimally. Structural and fabrication constrains limit the variation of percentage pitch to larger extents and hence a constant value of 82% has been implemented throughout the span.
- The tip profile of both fore and aft blade should represent a uniform tip gap. The tip shapes were derived by projecting the tip profiles of both fore and aft blade on a common cylindrical surface.

- The performance of rotor is highly sensitive to axial overlap. The change of axial overlap results in change of loading split between both blades, endwall-nozzle flow interaction and rotor passage vortex structure. These phenomena cumulatively dictate the rotor exit flow structure which is incident on the stator.
- Both load split and spanwise loading distribution are achieved as per the intended design till 70% span (for positive overlaps). The loading on the aft blade increases from hub to tip as prescribed. However, the load split is influenced in the tip regions due to tip clearance-nozzle flow interaction which influence the loading capability of aft blade. An important point worth noting is that there is quantitative increase in overall loading due to tandem effect but load split is as per the intended ratio to the maximum extent.

9.2. Design Aspects of Stator

- The flow incident on stator needs to undergo higher deflection due to expected higher rotor blade aerodynamic loading and axial exit velocity from the stage using a single stator blade. This result in higher stator blade turning along the span. This gets coupled with twin rotor wakes from the tandem rotor resulting in a challenging aerodynamic inflow structure faced by stator.
- In order to address the flow separation issue on stator suction surface, the innovative approach of using DCA camberline with controlled turning distribution has been implemented. The use of DCA camberline facilitates a precise control of chordwise flow field. A primarily fore - loaded configuration is suited for majority of the span location except near both endwalls.
- Based on systematic numerical study, it was realized the flow angle at the inlet of stator need to be reconsidered as per the exit flow coming from the twin rotor blades. The twin wake system from tandem bladed rotor results in an unconventional exit flow distribution from the tandem rotor. The wakes merge downstream of the rotor resulting in a thicker wake which changes the flow incidence on the stator.
- The extreme flow turning with expectations of axial flow exit result in tip and hub corner boundary layer complexities and it demands for specialized attention. This has been managed by incorporating endwall dihedral which provides the necessary radial pressure gradients to relieve endwall stator aerodynamic loading.
- Incorporation of dihedral results into migration of endwall flow more towards the midspan region. The current stator has high aerodynamic load in the midspan region due to twin wake impingement and peculiar inflow angle from tandem rotor. A precise dihedral distribution has been arrived at to limit this migration to optimum in order to avoid excess burden on core span.

ACKNOWLEDGMENT

This work has been done at Indian Institute of Technology Kharagpur. Authors would like to duly acknowledge **Sponsored Research and Industrial Consultancy (SRIC) IIT Kharagpur** for funding the research.

CONFLICT OF INTEREST

The authors declare that there is no conflict of interest.

REFERENCES

Alm-Eldien, A. M. (2015). Performance evaluation of the tandem c4 blades for axial-flow compressors. *American Journal of Aerospace Engineering*, *2*(1), 74. https://doi.org/10.11648/j.ajae.s.2015020101.17

Bammert, K., & Ahmadi, B. (1978). Investigations on impulse blade cascades with medium deflection. *Journal of Engineering for Power*, *100*(3), 432. https://doi.org/10.1115/1.3446375

Bammert, K., & Beelte, H. (1980). Investigations of an axial flow compressor with tandem cascades. *Journal of Engineering for Power*, *102*(4), 971. https://doi.org/10.1115/1.3230369

Bammert, K., & Staude, R. (1980). Optimization for rotor blades of tandem design for axial flow compressors. *Journal of Engineering for Power*, *102*(2), 369. https://doi.org/10.1115/1.3230263

Bammert, K., & Staude, R. (1981). *New features in the design of axial-flow compressors with tandem blades.* Volume 2: Coal, Biomass and Alternative Fuels; Combustion and Fuels; Oil and Gas Applications; Cycle Innovations, V002T08A012. https://doi.org/10.1115/81-GT-113

Belamri, T., Galpin, P., Braune, A. & Cornelius, C., (2005a). *CFD analysis of a 15 stage axial compressor: Part II — Results.* Turbo Expo 2005, Parts A and B, 1009–1017. https://doi.org/10.1115/GT2005-68262

Belamri, T., Galpin, P., Braune, A., & Cornelius, C. (2005b). *CFD analysis of a 15 stage axial compressor: Part I — Methods.* Turbo Expo 2005, Parts A and B, 1001–1008. https://doi.org/10.1115/GT2005-68261

Böhle, M., & Frey, T. (2014). Numerical and experimental investigations of the three-dimensional-flow structure of tandem cascades in the sidewall region. *Journal of Fluids Engineering*, *136*(7), 071102. https://doi.org/10.1115/1.4026880

Boroomand, M., Eshraghi, H., & M. Tousi, A. (2016). A developed methodology in design of highly loaded tandem axial flow compressor stage. *Journal of Applied Fluid Mechanics*, *9*(1), 83–94. https://doi.org/10.18869/acadpub.jafm.68.224.23948

Corsini, A., Delibra, G., & Sheard, A. G. (2013). A critical review of computational methods and their application in industrial fan design. *ISRN Mechanical*

Engineering, *2013*(327). https://doi.org/10.1155/2013/625175

Denton, J. D. (1993). *Loss Mechanisms in Turbomachines.* Combustion and Fuels; Oil and Gas Applications; Cycle Innovations; Heat Transfer; Electric Power; Industrial and Cogeneration; Ceramics; Structures and Dynamics; Controls, Diagnostics and Instrumentation; IGTI Scholar Award. https://doi.org/10.1115/93-GT-435

Duc Vo, H., Tan, C. S., & Greitzer, E. M. (2008). Criteria for spike initiated rotating stall. *Journal of Turbomachinery*, *130*(1). https://doi.org/10.1115/1.2750674

Eshraghi, H., Boroomand, M., & Tousi, A. M. (2014). *Design and analysis of a highly loaded tandem compressor stage.* Advances in Aerospace Technology, V001T01A071. https://doi.org/10.1115/IMECE2014-39750

Falla, G. A. C. (2004). *Numerical investigation of the flow in tandem compressor cascades* [Vienna university of Technology]. http://publik.tuwien.ac.at/files/pub-mb_2743.pdf

Frost, G. R., & Wennerstrom, A. J. (1973). *The design of axial compressor airfoils using arbitrary chamber lines.* Aerospace Research Laboratories, Air Force Systems Command, United States Air Force. https://doi.org/10.21236/AD0765165

Frost, G. R., Hearsey, R. M., & Wennerstrom, A. J. (1972). *A computer program for the specification of axial compressor airfoils.* Aerospace Research Laboratories, Air Force Systems Command, United States Air Force. https://doi.org/10.21236/AD0756879

Gallimore, S. J., Bolger, J. J., Cumpsty, N. A., Taylor, M. J., Wright, P. I., & Place, J. M. M. (2002). The use of sweep and dihedral in multistage axial flow compressor blading - Part II: Low and high-speed designs and test verification. *Journal of Turbomachinery*, *124*(4), 533–542. https://doi.org/10.1115/1.1507334

Hergt, A., & Siller, U. (2019, April, 1–9). About subsonic compressor tandem aerodynamics - A fundamental study. *Open Archives of the 16th International Symposium on Transport Phenomena and Dynamics of Rotating Machinery*, ISROMAC 2016.

Hoeger, M., Baier, R. D., Fischer, S., & Neudorfer, J. (2011). High turning compressor tandem cascade for high subsonic flows - Part 2: Numerical and experimental investigations. *Proceedings of 47th Joint Propulsion Conference*, *AIAA-2011-5601*, 1–14. https://doi.org/10.2514/6.2011-5602

Horlock, J. H. (2018). The determination of end-wall blockage in axial compressors : A comparison between Various Approaches. *Journal of Turbomachinery*, *122*(2), 218–224. https://doi.org/10.1115/1.555452

Inoue, M., & Furukawa, M. (2002). Physics of tip clearance flow in turbomachinery. *American Society of Mechanical Engineers, Fluids Engineering Division (Publication) FED*, *257*(2 B), 777–789. https://doi.org/10.1115/FEDSM2002-31184

Inoue, M., Furukawa, M., Saiki, K., & Yamada, K. (1998). Physical explanations of tip leakage flow field in an axial compressor rotor. *Proceedings of the ASME Turbo Expo*, *1*. https://doi.org/10.1115/98-GT-091

Jiang, M., Machiraju, R., & Thompson, D. (2005). Detection and visualization of vortices. *Visualization Handbook*, 295–309. https://doi.org/10.1016/B978-012387582-2/50016-2

Khalid, S. A., Khalsa, A. S., Waitz, I. A., Tan, C. S., Greitzer, E. M., Cumpsty, N. A., Adamczyk, J. J. & Marble, F. E. (1999). Endwall Blockage in Axial Compressors. *Journal of Turbomachinery*, *121*(3), 499–509. https://doi.org/10.1115/1.2841344

Koch, C. C. (1981). Stalling pressure rise capability of axial flow compressor stages. *Journal of Engineering for Power*, *103*(4), 645–656. https://doi.org/10.1115/1.3230787

Lei, V., Spakovszky, Z. S., & Greitzer, E. M. (2018). *A criterion for axial compressor hub-corner stall*. *130*(July 2008), 1–10. https://doi.org/10.1115/1.2775492

Levy, Y., Degani, D., & Seginer, A. (1990). Graphical visualization of vortical flows by means of helicity. *AIAA Journal*, *28*(8), 1347–1352. https://doi.org/10.2514/3.25224

Madasseri Payyappalli, M., & Pradeep, A. M. (2018). *Effect of tandem blading in contra-rotating axial flow fans. Volume 2A: Turbomachinery*, 1–12. https://doi.org/10.1115/GT2018-75477

Madasseri Payyappalli, M., & Shine, S. R. (2015). *Numerical investigation on tandem compressor cascades*. ASME 2015 Gas Turbine India Conference, V001T01A013. https://doi.org/10.1115/GTINDIA2015-1311

McGlumphy, J., Ng, W. F., Wellborn, S. R. & Kempf, S. (2010). 3D numerical investigation of tandem airfoils for a core compressor rotor. *Journal of Turbomachinery*, *132*(3), 031009. https://doi.org/10.1115/1.3149283

McGlumphy, J., Ng, W. F., Wellborn, S. R., & Kempf, S. (2009). Numerical investigation of tandem airfoils for subsonic axial-flow compressor blades. *Journal of Turbomachinery*, *131*(2), 021018. https://doi.org/10.1115/1.2952366

Mohsen, M., Owis, F. M., & Hashim, A. A. (2017). The impact of tandem rotor blades on the performance of transonic axial compressors. *Aerospace Science and Technology*, *67*, 237–248. https://doi.org/10.1016/j.ast.2017.04.019

Sakai, Y., Matsuoka, A., Suga, S., & Hashimoto, K. (2003). *Design and test of transonic compressor rotor with tandem cascade.* Proceedings of the International Gas Turbine Congress. 1–6.

https://nippon.zaidan.info/seikabutsu/2003/00916/pdf/igtc2003tokyo_ts108.pdf

Sakulkaew, S., Tan, C. S., Donahoo, E., Cornelius, C., & Montgomery, M. (2013). compressor efficiency variation with rotor tip gap from vanishing to large clearance. *Journal of Turbomachinery*, *135*(3), 031030. https://doi.org/10.1115/1.4007547

Sanger, N. L. (1971). *Analytical study of the effects of geometric changes on the flow characteristics of tandem-bladed compressor stators*. National Aeronautics and Space Administration.

Sanger, N. L. (1973). *Analytical study on a two dimensional plane of the off-design flow properties of tandem bladed compressor stators*. National Aeronautics and Space Administration.

Schluer, C., Böhle, M., & Cagna, M. (2009, March 23). Numerical investigation of the secondary flows and losses in a high-turning tandem compressor cascade. *8th European Conference on Turbomachinery: Fluid Dynamics and Thermodynamics, ETC 2009* - Conference Proceedings.

Schneider, T., & Kožulović, D. (2013). *Flow characteristics of axial compressor tandem cascades at large off-design incidence angles. Volume 6A: Turbomachinery*, *6 A*, V06AT35A011. https://doi.org/10.1115/GT2013-94708

Sheets, H. E. (1955). The slotted blade axial-flow blower. *The American Society of Mechanical Engineers*. http://oai.dtic.mil/oai/oai?verb=getRecord&metadataPrefix=html&identifier=ADA284605

Singh, A., & Mistry, C. S. (2019). *Study on effect of axial overlap on tip leakage flow structure in tandem bladed low speed axial flow compressor. Volume 2A: Turbomachinery*, *Volume 2A:* https://doi.org/10.1115/GT2019-91366

Singh, A., & Mistry, C. S. (2020). *Aerodynamic design aspects for stator of highly loaded tandem bladed axial compressor*. Proceedings of the ASME Turbo Expo, 2A-2020. https://doi.org/10.1115/GT2020-15968

Smith, A. M. O. (1975). High-lift aerodynamics. *Journal of Aircraft*, *12*(6), 501–530. https://doi.org/10.2514/3.59830

Smith, L. H., & Yeh, H. (1963). Sweep and dihedral effects in axial-flow turbomachinery. *Journal of Basic Engineering*, *85*(3), 401–414. https://doi.org/10.1115/1.3656623

Spraglin, W. E. (1951). *Flow through cascades in tandem*. National Advisory Committee for Aeronautics. https://ntrs.nasa.gov/citations/19930088962

Storer, J. A., & Cumpsty, N. A. (1991). Tip leakage flow in axial compressors. *Journal of Turbomachinery*, *113*(2), 252–259. https://doi.org/10.1115/1.2929095.

Tiralap, A., Tan, C. S., Donahoo, E., Montgomery, M. & Cornelius, C. (2017). Effects of Rotor Tip Blade Loading Variation on Compressor Stage Performance. Journal of Turbomachinery, 139(5), 1–11. https://doi.org/10.1115/1.4035252

Tao, Y., Wu, Y., Yu, X., & Liu, B. (2020). Analysis of flow characteristic of transonic tandem rotor airfoil and its optimization. *Applied Sciences (Switzerland)*, *10*(16). https://doi.org/10.3390/app10165569

Vad, J. (2008). Aerodynamic effects of blade sweep and skew in low-speed axial flow rotors at the design flow rate: An overview. *Proceedings of the Institution of Mechanical Engineers, Part A: Journal of Power and Energy*, *222*(1), 69–85. https://doi.org/10.1243/09576509JPE471

Wilcox, D. C. (2006). *Turbulence modeling for CFD*. DCW Industries. https://books.google.co.in/books?id=tFNNPgAACAAJ

Wisler, D. C. (1985). Loss reduction in axial-flow compressors through low-speed model testing. *Journal of Engineering for Gas Turbines and Power*, *107*(2), 354. https://doi.org/10.1115/1.3239730

Zhou, C., Zhao, S., & Lu, X. (2023). Investigating the aerodynamic design of a novel tandem fan with a partial-span booster rotor. *Aerospace Science and Technology*, *132*, 108018. https://doi.org/10.1016/j.ast.2022.108018